8

Nanostructured Composite Materials for CO_2 Activation

Anurag Kumar,[1,2] *Pawan Kumar*[1,2] and *Suman L. Jain*[1,*]

Introduction

Due to tremendous exploitation of natural fuel reserves to fulfil our energy demands, the concentration of green house gases has increased to manifold in the last few decades. A plethora of frequently released reports on climate change gives clear evidence of harmful impact on the environment due to anthropogenic emissions of greenhouse gases. The most easily accessible and widely exploited source of energy is hydrocarbon having high energy density (33 GJ/m^3 for gasoline) and is derived from fossil fuel (see Brand and Blok 2015, Johnson et al. 2007, Peura and Hyttinin 2011, Giesekam et al. 2014). Approximately 81% of energy comes from burning of fossil fuel while renewable source accounts for only 13% of the total energy produced. Among various green house gases, carbon dioxide (CO_2) has the most prominent effect on environment because it is a major component of emission (see Manne and Richels 2001, Panwar et al. 2011). The carbon dioxide (CO_2) concentration in the atmosphere has been rising steadily since the beginning of the industrial revolution. As a result, the current CO_2 level is the highest in at least the past 8,00,000 years (see Rehan and Nehdi 2005, Cempbell et al. 2008, Zachos et al. 2008, Wang et al. 2011). Due to this, the global earth temperature and sea level are continuously rising along with depletion of fossil fuel reserves. Various techniques for capturing and storing of CO_2 have been developed like in underground abandoned oil wells, storage under sea water, etc. (see Dincer 1999, Bachu 2008, Gouedard et al. 2009, Markewitz et al. 2012). But sudden spilling and acidification of sea water can deteriorate natural flora and fauna. Thus, conversion of CO_2 to high value chemicals is a promising option and in this regard, valuable products like polycarbonates, polyols esters, etc. have been synthesized from carbon dioxide (see Zhou et al. 2008, Aresta et al. 2014, Lanzafame et al. 2014, Olah et al. 2009). However, CO_2 is highly thermodynamically stable molecules and, therefore, its further conversion to value added chemical is energy intensive and requires heat and catalyst which add extra cost and makes process less viable for the realization of technology. Sunlight is an inexhaustible source of energy and can be used

[1] Chemical Sciences Division, CSIR-Indian Institute of Petroleum, Dehradun-248005, India.
[2] Academy of Scientific and Industrial Research (AcSIR), New Delhi-110001, India.
Emails: anukmnbd@gmail.com; choudhary.2486pawan@yahoo.in
* Corresponding author: suman@iip.res.in

for the production of solar fuel (see Momirlan and Veziroglu 2005, Barber 2009). The mean solar light irradiance at normal incidence outside the atmosphere is 1360 W/m^2, and the total annual incidence of solar energy in India alone is about 107 kW, and for the southern region, the daily average is about 0.4 kW/m^2. If we are able to harvest 10% of sunlight falling on 0.3% of earth's land surface, it will be sufficient to meet our energy demand by 2050 (see Cook et al. 2010, Jacobson et al. 2013, Powell and Lenton 2012). Hydrogen has been considered an ideal fuel with high calorific value and water is the only by-product of its combustion. But due to high mass to volume ratio storage, transfer of hydrogen is difficult (see Felderhoff et al. 2007, Atabani et al. 2012). Till date, most of the industrial hydrogen is produced by methane reforming of natural gas (see Barelli et al. 2008). Solar water splitting for hydrogen production can be a sustainable route for the production of hydrogen by the cheapest, widely available source water (see Krol et al. 2008, Peharz et al. 2007). However, the problem of storage still exists. Many adsorbing agents like hydrides, MOFs, etc. have been used for the storage of hydrogen via temporary bond formation but desorption from the surface requires high temperature that is disadvantageous in the viewpoint of energy. Chemical storage in the lower hydrocarbons or oxygenated hydrocarbons can solve the problem of hydrogen storage (see Davda et al. 2005, Dresselhaus and Thomas 2001). Photocatalytic reduction of CO_2 using water as a source of hydrogen to hydrocarbons is the most promising approach for levelling the concentration of greenhouse CO_2 along with the storage of hydrogen in the form of fuel (see Du et al. 2009, Roy et al. 2010). In this process, water splitting generates electrons and protons which are utilized for the reduction of CO_2 to hydrocarbons. This process is similar to photosynthesis where higher products are produced from water and CO_2, so this process is called artificial photosynthesis.

Since the discovery of photocatalytic water splitting over TiO_2 by Fujishima and Honda in 1972, a great deal of research has been focused on semiconductor photocatalysis (see Fujishima and Honda 1972). However, for the first time, Halmann (1978) reported that CO_2 can also be reduced electrochemically over GaP electrode by using UV light to various lower hydrocarbons, i.e., formic acid, methanol, methane, formaldehyde, etc. (Halmann 1978). After that, Inoue et al. (1979) used various semiconductors like WO_3, TiO_2, ZnO, CdS, etc. for CO_2 reduction by using Xe lamp. Most of the identified products were C1 products (Inoue et al. 1979). These initial findings have opened path for using various semiconductor materials like ZnS, CdS, Cu_2O, ZnO, Fe_2O_3, WO_3, etc. for efficient reduction of CO_2 to valuable products (see Mao et al. 2013, Li et al. 2014, Navalon et al. 2013, Neaţu et al. 2014). It has been observed that semiconductors mainly produce formic acid, CO and methane. Gaseous products are less desirable because of the problem associated with their storage. Among the all liquid products formed, methanol has been identified as the best liquid C1 oxygenates because of high calorific value, higher octane number and suitability to internal combustion engines (see Ganesh 2014).

Basic principle of CO_2 reduction

The reduction of CO_2 is highly unfavourable because of its linear geometry and closed shell structure which makes it highly stable (Heat of formation ΔH^o gas = –393.5 KJ/mol). One electron reduction of CO_2 to CO_2^{-o} radical is highly unfavorable because of generation of bent structure in which acquired additional electron imposes repulsive force on lone pair of electrons at oxygen atoms. This arrangement makes the one electron reduced species highly unstable which requires high reduction potential (–1.90 V vs. NHE) (see Zhang et al. 2004, Balcerski et al. 2007, Wang et al. 2009a). Although proton-assisted multiple-electron transfers (MET) is a much easier way to reduce CO_2 at lower reduction potential than one electron reduction (see Tahir and Amin 2013, Xiang et al. 2011, Liu et al. 2010a). It can be seen from Eqs. 1–7 that proton assisted reduction can be achieved at lower reduction potential. Further for getting hydrocarbons with higher C:H ratio, transfer of multiple electrons and protons is essential. The required electrons and protons can be obtained from water oxidation or water splitting (H_2O/O_2 (+0.82 V vs. NHE at pH 7).

$$CO_2 + 2H^+ + 2e^- \rightarrow CO + H_2O \qquad E^0 = -0.53\ V \ldots\ldots\ldots\ldots \quad (1)$$

$$CO_2 + 2H^+ + 2e^- \rightarrow HCOOH \qquad E^0 = -0.61\ V \ldots\ldots\ldots\ldots \quad (2)$$

$$CO_2 + 4H^+ + 4e^- \rightarrow HCHO + H_2O \qquad E_0 = -0.48\ V \ldots\ldots\ldots\ldots \quad (3)$$

$$CO_2 + 6H^+ + 6e^- \rightarrow CH_3OH + H_2O \qquad E^0 = -0.38\ V \ldots\ldots\ldots\ldots\ldots \quad (4)$$

$$CO_2 + 8H^+ + 8e^- \rightarrow CH_4 + 2H_2O \qquad E^0 = -0.24\ V \ldots\ldots\ldots\ldots\ldots \quad (5)$$

$$CO_2 + e^- \rightarrow CO_2^{-o} \qquad E^0 = -1.90\ V \ldots\ldots\ldots\ldots\ldots \quad (6)$$

$$2H^+ + 2e^- \rightarrow H_2 \qquad E^0 = -0.41\ V \ldots\ldots\ldots\ldots\ldots \quad (7)$$

The reduction potential of CO_2/CH_3OH is –0.38 V (at pH 7 vs. NHE), while for reducing proton to hydrogen, the value is 0.00 V at pH-0. However, –0.41 V over potential is needed for the production of hydrogen in aqueous solutions at pH 7 vs. NHE (H^+/H_2 (–0.41 V vs. NHE at pH-7). Because the values of reduction potential for proton reduction and CO_2 reduction are almost similar, so the photocatalyst that can reduce CO_2 can also reduce protons (see Izumi 2013, Sato et al. 2015). Therefore, hydrogen is always observed as a by-product which makes the process less efficient because protons compete for the electrons.

It is noteworthy to mention here that the reduction potential changes by changing pH value according to Nernst equation (Eq. 8).

$$E^0\,(pH) = E^0\,(pH0) - 0.06pH \ldots\ldots\ldots\ldots\ldots\ldots\ldots \quad (8)$$

Semiconductor materials work as photocatalyst due to the presence of band gap. The band gap of semiconductors is determined by the energy difference between hybridized system of HOMO (highest occupied molecular orbital) and LUMO (lowest unoccupied molecular orbital) of the material (see Wehling et al. 2008, Ajayaghosh 2003). In semiconductors, after absorption of light of appropriate wavelength, electrons get excited from valance band to conduction band which creates positively charged vacancy in valance band (holes) (see Chestnoy et al. 1986). Electrons can reduce any species while holes are responsible for the oxidation (see Dukovic et al. 2004).

For the efficient water splitting or CO_2 reduction, the band gap of semiconductor should be higher than 1.23 V. In other words, the position of valance band should be more positive than +0.82 V vs. NHE at pH-7, so it can oxidize water while the position of conduction band should be more negative than –0.41 V vs. NHE at pH-7, so it can reduce CO_2 or protons (see Karamian and Sharifnia 2016). Very few semiconductors meet this requirement of suitable band position and most of the semiconductors have wide band gaps and absorb in the UV region. However, the solar spectrum consists of only about 4% of UV light (see Nagaveni et al. 2004, Kumar and Devi 2011, Hashimoto et al. 2005), but of about 45% visible light, so the basic need is to develop photocatalyst that can absorb in visible region. Further, charge recombination is a prominent phenomenon in the semiconductors which is also responsible for lowering the photo-efficiency (see Hochbaum and Yang 2010, Yu et al. 2010). Only less than 10% of produced electron and protons are available for the water splitting or CO_2 reduction process. The recombination may be of two types, i.e., the volume recombination and surface recombination (see Linsebigler et al. 1995). Volume recombination can be prevented by reducing the particles size of semiconductor so more electrons and holes can reach at the surface while surface recombination can be stopped by electron and hole capturing agents like doping with metals. Doping with various metals like Cu, Ag, Au, Pt, Ru etc. and non-metals like C, N, S, I, etc. can be a viable approach for reducing the fast electron hole recombination along with band gap modification (see Zhang et al. 2013, Kumar and Devi 2011). Doped metal has Fermi level below the conduction band of semiconductor so it can accept electrons efficiently. Due to this effect, the Fermi level of semiconductor shifts slightly upward and semiconductor becomes more reductive in nature. Back transfer of electron may reduce catalytic performance, so reducing the size of semiconductor material can slow down the process of back electron transfer. Some metal oxides like IrO_2, CoO_x can capture holes (see Zhong et al. 2011, Li et al. 2013a, Wang et al. 2015b). Non-metal dopants like B, C, N, S, etc. have 2p orbital with higher energy than O 2p orbital in TiO_2, so hybridization of these orbital generates a new hybridized orbital with higher energy and the valance band position shifts to higher energy (less positive). This resulted to the lowering of band-gap and therefore material can absorb in the visible region. Wu et al. (2011) reported that the band gap of N doped and N–B co-doped TiO_2 was 2.16 eV and 2.13 eV, respectively (Zhang et al. 2011a), which is much smaller than that of pure TiO_2 (3.18 eV for anatase) (see Serpone et al. 1995). Further, reduction of semiconductor in hydrogen at higher temperature creates vacancy due to abstraction of oxygen atom which creates colour centre and

material can absorb in the visible region (see Varghese et al. 2009, Wang et al. 2010). Apart from electron and hole capturing agents, sacrificial donors can be added for getting higher yield of CO_2 reduction products. Tertiary amines like triethylamine, triethanolamine, BNAH and NaOH, Na_2SO_3, Na_2S, EDTA, etc. have been used as sacrificial agents.

Most of the semiconductors, due to the inappropriate position of their band edge position, can initiate either water splitting or CO_2 reduction only. Very few semiconductors like TiO_2 ZnS, ZnO, etc. meet the demand of suitable band edge position but their large band gap limits their application (see Pradhan and Sharma 2011, Choudhary et al. 2012). This limitation can be overcome by synthesizing heterojunctions by mixing of low band gap semiconductors with high band gap semiconductors in which one can reduce CO_2 and other can oxidize water. This addition creates a p-n heterojunction and photogenerated electrons and holes can move from low band gap semiconductor to high band gap semiconductor. Low band gap semiconductor can transfer electron to the high band gap semiconductor via two mechanisms in which the first mechanism is direct and the second is Z-scheme depending on band edge position of high band gap semiconductors (see Yang et al. 2012, Qu and Duan 2013, Wang et al. 2013a). In direct scheme, low band gap semiconductor, after absorption of visible light, transfer electrons and holes to high band gap semiconductor and indirectly produce charge separated species at high band gap semiconductor. While in Z scheme, a semiconductor which can only oxidize water gets excited by absorption of photon, so the generated electrons move to its conduction band while holes are used for oxidation of water (see Takanabe and Domen 2012). However, due to lower position of conduction band, they cannot reduce CO_2. So electrons in conduction band are transferred to valance band of another semiconductor which has

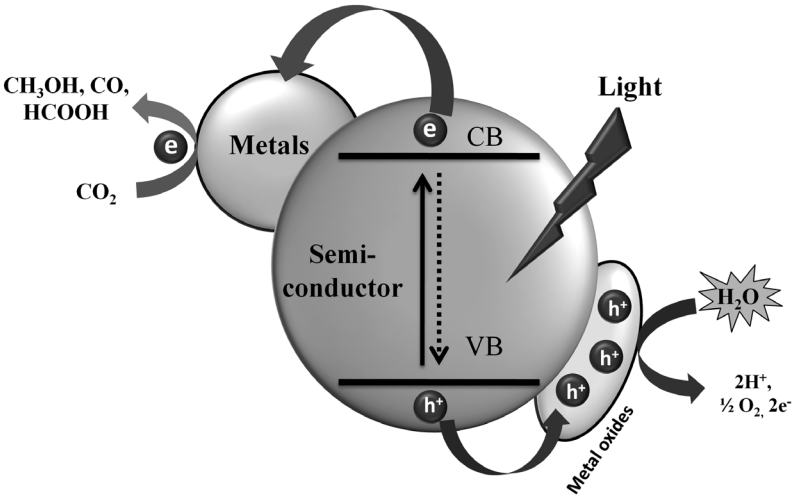

Figure 1. Mechanism of electrons and holes capture by metal and metal oxides doped semiconductor.

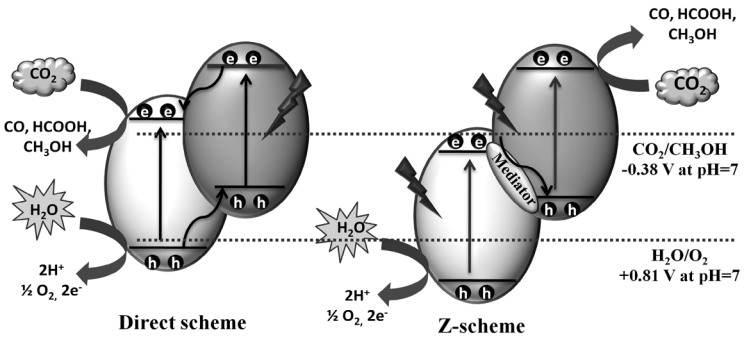

Figure 2. Schematics of CO_2 reduction and water oxidation over direct scheme and Z-scheme photocatalytic systems.

higher position of valance band (see Wang et al. 2015a). Generally, in electron mediator redox system like IO_3^-/I^-, Fe^{3+}/Fe^{2+}, $[Co(bpy)_3]^{3+/2+}$, etc. redox couples are required in Z scheme photocatalysis which play an important role in transfer of electrons from water oxidation photocatalyst to CO_2 reduction catalyst. For example, Z-scheme photosystem composed of $Pt/SrTiO_3$:Rh as hydrogen evolving catalyst and $BiVO_4$ as oxygen evolving catalyst was visible light responsive in the presence of Fe^{3+}/Fe^{2+} redox couple and can operate under 520 nm wavelength, which corresponds to the band gap of $SrTiO_3$:Rh and $BiVO_4$ (see Konta et al. 2004). In some cases, nanoparticles and conductive graphene sheets have been reported to work as electron mediator which facilitates better charge transfer (see Brownson et al. 2011, Yang et al. 2014). For example, in their work, He et al. (2015) used $Ag_3PO_4/g\text{-}C_3N_4$ composites for CO_2 reduction which works as Z-scheme photocatalyst and *in situ* generated Ag nanoparticles that work as electron facilitator (He et al. 2015). In this system, Ag_3PO_4 transfer electron to the valance band of carbon nitride via exited state and carbon nitride, after absorption of photon, transfer electrons to conduction band which are used for the CO_2 reduction while holes in valance band of $AgPO_4$ are used for water oxidation. The optimal $Ag_3PO_4/g\text{-}C_3N_4$ photocatalyst gave CO_2 reduction rate of 57.5 μmol h^{-1} $gcat^{-1}$, which was 6.1 and 10.4 times higher than $g\text{-}C_3N_4$ and P25, respectively. Another work by Iwase et al. (2011) used $BiVO_4$ and $Ru/SrTiO_3$:Rh Z scheme photocatalyst in which photoreduced graphene oxide (PRGO) work as solid electron mediator (Iwase et al. 2011).

Oxides based nanostructured composite for CO_2 reduction

Various semiconductors and their composites are extensively studied for the photocatalytic reduction of CO_2. Among them, titanium oxide (TiO_2) is the most widely used because of its abundance, nontoxic nature, wide band gap, non corrosive nature and higher activity (see Takayama et al. 2017, Qu and Duan 2013). TiO_2 is found in two main forms in which the first one, anatase, has tetragonal geometry where Ti^{+4} ions are surrounded by O^{-2} ions in octahedral manner and the second one is rutile form having slightly orthorhombic distortion (see Izumi 2013). Owing to this distortion, TiO_2 has different band gap in both anatase and rutile form. The band gap of anatase TiO_2 is 3.2 eV associated with 389 nm wavelength while the band gap of rutile form is 3.0 eV associated with 413 nm wavelength. In natural P25 TiO_2, both anatase and rutile forms exist in the ratio of 80:20 with particle size 25 nm and 56 m^2 g^{-1} BET surface area. Rutile form is more stable at higher temperature and annealing at temperature above 400ºC promotes the transformation of anatase to rutile form. Surprisingly, anatase form is more photoactive in comparison to rutile, which has low band gap because the charge recombination rate is 10 times slower in anatase form. It has been found that mixture of rutile and anatase form was more photoactive in comparison to individual component that was assumed due to transfer of electrons from CB of anatase form to CB of rutile form. However, in some literatures, it has been proposed that in anatase form trapping sites are present at 0.8 eV below the conduction band and electrons can flow from CB of rutile to anatase. Anatase TiO_2 has CB band edge position –0.58 V (vs. NHE at pH-7), so it can reduce CO_2 while VB position is +2.52 V (vs. NHE at pH-7) which facilitates water oxidation (see Kondratenko et al. 2013).

In TiO_2, some physical properties like adsorption, catalytic reactivity, selectivity, etc. were determined by surface atomic configuration and the degree of exposure of reactive crystal facets. Typically, during the synthesis of anatase TiO_2, higher energy facets {001} (0.90 J/m^2) get diminished quickly and the crystals are dominated by the thermodynamically stable {101} facets with lower surface free energy (0.44 J/m^2). Normal synthesis conditions produce truncated octahedral bipyramid (TOB) seed, exposing eight {101} facets and two {001} facets. However, high-energy {001} facets can be stabilized by the use of capping agents typically fluorides (see Liu et al. 2011, Yang et al. 2009, Yang et al. 2008, Liu et al. 2010d). The {001} facet anatase TiO_2 was found to be more active for the reduction of CO_2. So increasing the {001} facet should drive more CO_2 reduction products. But contradictory to a report by Yu et al. (2014a), the 58% {001} facet TiO_2 was found to be more active for CO_2 reduction in comparison to 83% {001} facet TiO_2. The highest rate of methane production obtained for HF 4.5 is 1.35 μmol g^{-1} h^{-1}. The possible reason of increased yield was explained on the basis of energy difference ("surface heterojunction") determined by DFT calculation. It has been found that CB and VB position of {101} facet TiO_2 is lower in energy than {001} facet TiO_2 so photogenerated electrons can move from the conduction band of {001}

facet TiO_2 to {101} facet TiO_2 while hole moves in opposite direction (Yu et al. 2014a). Similarly, {111} facet TiO_2 has much higher energy (1.61 J/m^2) that arises from the under coordinated Ti atoms and O atoms that existed on the {111} surface which acts as active sites in the photoreaction (see Sun et al. 2011, Liu et al. 2012). Experimentally, it has been proved that {111} facet TiO_2 is the most photoactive among other TiO_2 samples exposed with majority {010}, {101}, and {001} facets (see Xu et al. 2013a). A less explored form of anatase TiO_2, the {100} facet having intermediate energy (0.44 J/m^2) is considered to be the best attractive active facet because of its superior surface atomic structure and electronic structure (see Li and Xu 2010, Pan et al. 2014, Li et al. 2012). Theoretical prediction reveals that the {100} facet should appear as the "belt"; however, in most of cases single crystals with exposed {100} facet, anatase TiO_2 was obtained as rods or cuboids. The cuboids structure has {001} and {101} facet exposed on the upper and bottom of the cuboids. Apart from this, the small surface area as the utmost important property also limits their application. So the promising approach to increase surface area and {100} facet is to reduce the thickness of the TiO_2 cuboids which resulted in the decrease in the percentages of the {101} and {001} facets. In a report, Xu et al. (2013b) has synthesized ultrathin anatase TiO_2 nanosheets with high percentage of the exposed {100} facet and surface area (57.1 m^2 g^{-1}). The photoactivity of {100} facet TiO_2 sheets T_{Sheets} (362 μmol h^{-1}) was found to be about 3.5 times higher than $T_{Cuboids}$ (104 μmol h^{-1}) (Xu et al. 2013b).

Doping with various dopants further improve the photocatalytic character which also prevent the electron hole annihilation. For example, photochemically sensitive iodine-doped TiO_2 nanoparticles as synthesized by hydrothermal method were found to be active in visible light irradiation (see Zhang et al. 2011b). The photocatalytic activities of the I-TiO_2 powders were investigated for photocatalytic reduction of CO_2 with H_2O under visible light ($\lambda > 400$ nm) and also under UV–vis illumination. The photoreduction experiment showed that CO was a major photoreduction product (highest CO yield equivalent to 2.4 mol g^{-1} h^{-1}) which was much higher as compared in undoped TiO_2. In case of Cu/TiO_2 synthesized by improved sol-gel method, using $CuCl_2$ was found to be more active than Cu/TiO_2 synthesized by $(CH_3COOH)_2Cu$ for reduction of CO_2 to methanol. TPR, XPS, and XAS measurements showed that Cu(I) served as an active site. Further, higher zeta potential at pH 7 was found to be responsible for increased activity. The yield of methanol was found to be 600 μmol g^{-1} cat after 30 hr under UVC (254 nm) irradiation (see Tseng et al. 2004). Other semiconductors like ZnO, Fe_2O_3, CdS, ZnS, Nb_2O_5, Ta_2O_5, and $BiTaO_4$ have been explored as photocatalysts. In particular, oxides with perovskite structure formed by TaO_6 or NbO_6 octahedra layers have shown photocatalytic activity in tantalates and niobates of structural formula $NaMO_3$ (M = Ta and Nb) for the stoichiometric decomposition of water. Photocatalytic activity better than TiO_2 has been observed on laminar oxides such as $BaLi_2Ti_6O_{14}$, $MTaO_3$ (M = Li, Na, K), and SrM_2O_7 (M = Nb, Ta) for the degradation of organic pollutants. Some mixed oxides such as $In_{1-x}Ni_xTaO_4$, $CaIn_2O_4$, $InVO_4$, $BiVO_4$, and Bi_2MoO_6 have shown better visible light driven catalytic activity. In recent years, oxynitride solid-solution photocatalysts, such as $(Ga_{1-x}Zn_x)(N_{1-x}O_x)$ and $(Zn_{1+x}Ge)(O_xN_2)$, are established to be most efficient photocatalysts that work under visible-light irradiation (see Jensen et al. 2008, Chouhan et al. 2013). Although ZnO is a wide band gap (3.37 eV) material that is less investigated than TiO_2 for photocatalytic application, but in recent years it has emerged as an interesting alternative due to its photocatalytic activity, long lived charged species, low cost and noncorrosive nature (see Das and Khushalani 2010, Georgekutty et al. 2008). For reducing band gap, nitrogen doped ZnO (N-ZnO) nanobundles with visible-light photocatalytic activity has been synthesized by thermal treatment of ZnOHF nanobundles under NH_3 (see Zong et al. 2013). X-ray photoelectron spectroscopy (XPS) analysis indicated that N was bound to Zn as nitride (Zn-N) and oxynitride (O-Zn-N). The band gap of ZnO was reduced from 2.20 to 1.95 eV as a consequence of nitrogen doping which raises the VB position upward. Water splitting reaction was tested to check the performance of photocatalyst under visible light irradiation ($\lambda > 420$ nm) which showed significant increase in the rate of hydrogen evolution. Wang et al. (2014) synthesized the films of N-ZnO by reactive magnetron sputtering (Wang et al. 2014). The undoped ZnO films exhibited n-type conduction, while the N-ZnO films showed p-type conduction. N was involved mostly in Zn-N bonds, substituting O atoms to form NO acceptors in the N-ZnO films which were also confirmed by XPS analysis. The ZnO:N film has high optical quality and displays a stronger near band edge (NBE) emission in the temperature-dependent photoluminescence spectrum.

Porous nature of these materials is beneficial for enhanced concentration of CO_2 adsorbed on catalyst's surface which enhances yield of CO_2 reduction products due to access of more active sites. Park et al. (2012) has synthesized highly porous gallium oxide (Ga_2O_3) with mesopores and macropores by using TTAB (Myristyltrimethylammonium bromide) and utilized for the reduction of CO_2. The calculated surface area was found to be 42.7 m^2 g^{-1} as determined with BET. The amount of methane in the absence of any dopant found after 10 hr was found to be 2.09 μmol g^{-1} or 156 ppm which was much higher than Ga_2O_3 prepared without any template (Park et al. 2012).

Mixed nanostructured materials for CO_2 reduction

Nanoscale integration of multiple functional components in which one having low band-gap and another having high band-gap is beneficial because it increases the lifetime of excited state indirectly by continuous supply of electrons in the conduction band and providing holes in the valence band (see Chang et al. 2014). Careful designed core shell structure of two or more different semiconductors has proven a better photocatalyst because of better interfacial contact which facilitates better charge separation. For example, Ni@NiO core shell structure-modified nitrogen-doped $InTaO_4$ (Ni@NiO/$InTaO_4$-N) was found to be better catalyst for reduction of CO_2 to methanol (see Tsai et al. 2011). After 2 hr, the yield of methanol was found to be 350 μmol g^{-1} cat. Despite that, the CB of NiO (E_{CB} = –0.96 V vs. NHE) is more negative than $InTaO_4$ (ECB = –0.8 V vs. NHE), so the electron transfer from $InTaO_4$ to NiO is thermodynamically not possible, but modification with Ni double layered structure assists the transfer of photogenerated electrons to CB of $InTaO_4$ (see Kato and Kudo 2003). Pan et al. (2007) reported that nickel oxide working as a co-catalyst deposited on the surface of $InTaO_4$ and 1 wt% loading was optimal concentration used in the photoreduction of CO_2 to CH_3OH which afforded 1.394 μmol g^{-1} h^{-1} of methanol in the first 20 hr (Pan and Chen 2007). Lee et al. (2010) synthesized $InNbO_4$ modified with NiO and Co_3O_4 by incipient-wetness impregnation method and used for the CO_2 activation (Liu et al. 2010b). The 0.5 wt% NiO loaded $InNbO_4$ gave methanol up to 1.577 μmol g^{-1} h^{-1} cat while 0.5 wt% Co_3O_4 loaded $InNbO_4$ gave 1.503 μmol g^{-1} h^{-1} of methanol (see Lee et al. 2012). Wang and co-workers (2010) synthesized CdSe quantum dot sensitized TiO_2 and the Pt were incorporated by the wet impregnation methods onto the TiO_2 for the photoreduction of CO_2 to CH_3OH, CH_4, H_2 and CO as the secondary product in visible light (Wang et al. 2010). Liu et al. (2010c) has shown that ternary metal oxide like zinc orthogermanate (Zn_2GeO_4) can reduce CO_2 into methane. The yield was further increased by addition of 1 wt% RuO_2 and 1 wt% Pt nanoparticles (Liu et al. 2010c). In a report by Feng et al. (2010), ultrafine Pt nanoparticles supported on hollow TiO_2 nanotubes were synthesized *in situ* by microwave-assisted solvothermal approach. For Pt nanoparticles loaded, nanotubes' photocatalytic methane production rate of 25 ± 4 ppm/(cm^2 h) was obtained from the CO_2/water vapour atmosphere (see Feng et al. 2011, Xie et al. 2015). In another study by Yan et al. (2012), $ZnAl_2O_4$-modified mesoporous ZnGaNO solid solution was synthesized by a two-step reaction template route (Yan et al. 2012). The first step involves $NaGa_{1-x}Al_xO_2$ solid solution, which was prepared by heating the mixed gel of $NaGaO_2$ and $NaAlO_2$; however in the second step, $Zn(CH_3COO)_2$ aqueous solution was introduced into the $NaGa_{1-x}Al_xO_2$ colloidal suspension. The ion exchange reaction produced $ZnAl_2O_4$ modified mesoporous ZnGaNO after nitridation step. The $ZnAl_2O_4$-modified mesoporous ZnGaNO loaded with 0.5 wt% Pt as the co-catalyst exhibited a CH_4 generation rate of 9.2 μmol g^{-1} h^{-1} after 1 hr of visible light illumination ($\lambda \geq 420$ nm). BET and TPD results showed that high surface area and higher adsorption of CO_2 on catalyst surface promoted higher yield. Hollow nanotubes or other hollow structures possess superior photocatalytic performance because of low recombination in bulk volume. However, their design and structure are difficult to maintain. In another study, CuO-$TiO_{2-x}N_x$ hollow nanocubes with exceptionally high photoactivity were synthesized for reduction of CO_2 to CH_4 under visible light irradiation (see In et al. 2012). The yield of methane was found to be 41.3 ppm g^{-1} h^{-1} which was 2.5 times higher than that of Degussa P25 TiO_2 (16.2 ppm g^{-1} h^{-1}).

Layered double hydroxides (LDHs) with a general formula $[M^{2+}_{1-x}M^{3+}_x(OH)_2]^{x+}(A_n)_{x/n}\cdot mH_2O$) in as such form or after modification with different ions like M^{2+} = Mg^{2+}, Zn^{2+}, Ni^{2+}; M^{3+} = Al^{3+}, Ga^{3+}, In^{3+}, etc. were also investigated for the CO_2 reduction. For example Teramura et al. (2012) used Mg-In LDH as photocatalyst, which yields CO and O_2 (3.21 and 17.0 μmol g^{-1} h^{-1}, respectively) from 100 mg of Mg-

In LDH (Teramura et al. 2012). Ahmed and coworkers reported the use of various LDHs incorporated with different metal ions like Cu, Zn, Al, Ga, etc. for reduction of CO_2 at pressurized reactor under UV-Vis light irradiation. By using $[Zn_{1.5}Cu_{1.5}Ga(OH)_8]^+{}_2[Cu(OH)_4]^{2-}{\cdot}mH_2O$ (Zn-Cu-Ga) layered double hydroxides as photocatalyst, the yield of methanol was found to be 170 nmol g^{-1} cat h^{-1} (see Ahmed et al. 2011). Further addition of light absorbers can increase the yield of the products. In this context, Hong et al. (2014) synthesized LDHs modified with carbon nitride (Mg-Al-LDH/C_3N_4) for the photocatalytic reduction of CO_2. The nitrate ions were replaced with carbonates which facilitates CO_2 concentration over LDHs while carbon nitride generates electron hole pairs (Hong et al. 2014).

Sensitization of semiconductors with metal complexes

For enhancing the visible light absorption, other methods like sensitization with metal complexes can be used as light harvesting units (see Kumar et al. 2012). Homogeneous photocatalysts, including transition metal complexes such as ruthenium(II) polypyridine carbonyl complex, cobalt(II) trisbipyridine, and cobalt(III) macrocycles have been widely investigated for this reaction. Transition metal based molecular complexes are advantageous due to their high quantum efficiencies and high selectivity of products. However, transition metal complexes suffer from the drawback of non-recyclability and higher costs which limit their practical applications. In order to overcome these limitations, immobilization of transition metal complexes to a photoactive support is a promising approach as it provides facile recovery, recyclability as well as enhanced activity due to synergistic effect of both components. Metal complexes after absorption of visible light get excited via MLCT (metal to ligand charge transfer) transition and can transfer electrons to the conduction band of semiconductors which are used for the reduction of CO_2 or protons. For the efficient transfer of electrons from metal complex molecule to semiconductor, the position of LUMO of the metal complex should be higher in energy than the conduction band edge of the semiconductor. However, its rate depends on a number of parameters such as the orientation and distance of the light absorbing unit with respect to the surface or size and flexibility of the anchoring unit. The positively charged metal complex that is generated gets back to its initial state by extracting electrons from the valence band (or by transferring positive charge in valance band). So, the hole is created in the valance band of semiconductor which oxidizes water to derive necessary electrons and protons. Immobilization of metal complexes indirectly generates electron and hole pairs in the conduction band and valance band, respectively.

So far, a number of photosensitizers such as ruthenium polyazine, metal phthalocyanines, porphyrines, etc. have been used widely for the immobilization on photoactive semiconductor supports. For the efficient sensitization, the life time of excited state should be long enough to transfer electrons

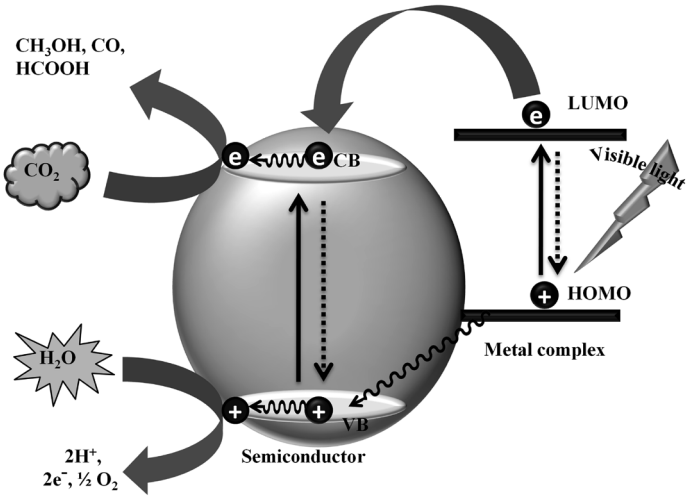

Figure 3. Basic illustration of CO_2 reduction by metal complexes sensitized photocatalyst.

in the conduction band of semiconductors. In this regard, nature of metal ions play a pivotal role for determining the life time of excited state; for example, tin phthalocyanine has longer life time of excited state than other metal phthalocyanines. So, there is sufficient time available for the transfer of electrons from the phthalocyanine molecule to the conduction band of semiconductor. Another major factor that influences electron transfer is the vicinity of metal complex with semiconductor. Attachment with linkers having long alkyl chain is less efficient in comparison to complexes attached with short chain linkers. Similarly, if metal complex is coordinated with semiconductor via a group having conjugated linker, the electron transfer from metal complex to conduction band is faster. But back electron transfer may be a detrimental process, so presence of sacrificial donor is of utmost importance which prevents the back transfer of electrons via donating electrons through redox quenching.

In general, semiconductor photocatalysts provide hydrocarbon products having lower C:H ratio (< 0.5) because of cessation of reaction on the surface of catalyst. So, in order to produce hydrocarbons with higher C:H ratio (> 0.5), multi-electron transfer is essential. The multi-electron transfer is possible by sensitization of semiconductors with molecular catalysts, which have the ability to generate more than one electron-hole pair simultaneously (see Mohamed and Bahnemann 2012).

Mainly, two approaches for the immobilization of metal complexes on the semiconductor supports have been utilized; the first one is non-covalent immobilization and the second one is covalent attachment. In a non-covalent approach, the metal complex can be immobilized to support material by ionic interaction, physical adsorption via van-der-Waals forces or through π–π interaction. Simple adsorption by van-der-Waals or π–π interaction of metal complex is less robust due to the weak interaction between support material and metal complex, so leaching of the catalyst from the solid support is an obvious drawback. Ionic interaction is somewhat stronger but ionization in the aqueous reaction medium limits its practical utility. Thus, covalent immobilization of metal complex to support is more attractive in the viewpoint of stability. For the covalent attachment of complex to the support, the surface of semiconductor should have lots of functionalities to accommodate enough concentration of metal complex. Furthermore, most of the semiconductor surface is decorated with –OH groups that form M-OH groups which are weaker than C-OH group; hence, multi-site attachment is more favourable to achieve highly stable photocatalysts. In this regard, the use of linkers provides benefits of strong and leaching proof multisite attachment of metal complex to the solid support matrix. The most commonly used linkers are 3-aminopropyl trimethoxysilane (APTMS), dopamine, glycine, etc. Furthermore, the stability of any immobilized complex on semiconductor is strongly dependent on the number of sites and nature of groups through which it is coordinated.

O. Ishitani and co-workers have done lot of work in the field of immobilization of homogeneous metal complexes of ruthenium $[Ru(dcbpy)(bpy)(CO)_2]^{2+}$, rhenium $[Re(dcbpy)(CO)_2]^{1+}$, etc. on various semiconductor supports like tantalum oxynitride, carbon nitride, etc. In a recent work, Sato et al. linked $[Ru\text{-}(dcbpy)_2(CO)_2]^{2+}$ complex, N-doped Ta_2O_5 ($N\text{-}Ta_2O_5$) as a p-type semiconductor for the photoreduction of CO_2 under visible light and obtained HCOOH selectively with a TON value of 89 (see Yamanaka et al. 2011). Here the p-type semiconductor is beneficial since it fastens the transport of electrons to the complex. Recently, Woolerton et al. (2010) developed ruthenium complex sensitized TiO_2 attached enzymatic system in which Ch-CODH I: carboxydothermus hydrogenoformans, expressed as carbon monoxide dehydrogenase, were able to transfer two electrons simultaneously to the CO_2 (Woolerton et al. 2010). This enzyme coupled catalytic system was used to reduce CO_2 to CO selectively. Sekizawa et al. (2013) reported Ru metal complex attached with semiconductor for the photocatalytic reduction of CO_2 to CH_3OH, HCOOH via Z-scheme mechanism (Sekizawa et al. 2013).

It has been well documented in the literature that phthalocyanines have a longer life time of excited state in comparison to ruthenium complex so they can effectively transfer electrons to semiconductors. In this regard, recently Kumar et al. (2015a) have synthesized tin phthalocyanine dichloride ($SnPcCl_2$) immobilized to mesoceria ($SnPc@CeO_2$) by considering the labile chlorine atoms as the linking sites (Kumar et al. 2015a). It has been observed that in the solution form, SnPc remains in agglomerated form and gives broad Q band from 650 nm to 750 nm while after attachment to meso-ceria support, it converted to monomeric form and gave sharp Q band which is a clear indication of attachment of SnPc to mesoceria. The synthesized photocatalyst was used for the visible light assisted photoreduction of CO_2

to methanol along with minor amount of CO and H_2 using triethylamine as sacrificial donor. By using SnPc@CeO_2, the yield of methanol, CO and H_2 was found to be 2342 μmol g^{-1} cat, 840 mmol g^{-1} cat and 13.5 mmol g^{-1} cat after 24 hr of vis-irradiation. However, it has been observed that after a certain period, the rate of methanol formation started to deplete that was due to consumption of CO_2 in the reaction mixture. In order to confirm that the saturation point is reached due to consumption of CO_2 and not due to the deactivation of the photocatalyst, the reaction mixture was re-purged with CO_2 and again irradiated under visible light. The yield of methanol again increased which confirmed that the photocatalyst was not deactivated during irradiation.

The higher photocatalytic performance was explained on the basis of better electron injection from SnPc to conduction band of mesoceria. After absorption of visible light, SnPc get excited via MLCT transition and electrons get transferred from HOMO to LUMO. This excited state transfers electrons to the conduction band of CeO_2. Triethylamine works as sacrificial donor and get degraded to its degradation products like acetaldehyde and diethyl amine, etc.

In recent years, magnetically separable nanocomposite materials have gained considerable attention because of the easy recovery of the catalyst after reaction by using external magnet. In this regard,

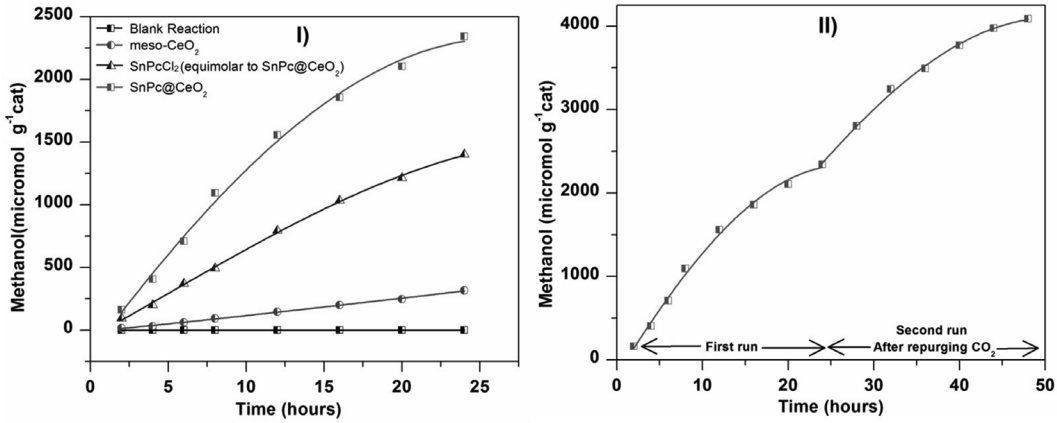

Figure 4. (I) Photocatalytic methanol formation versus time by using (a) blank reaction, (b) meso-CeO_2 and (c) $SnPcCl_2$ equimolar amount as in SnPc@CeO_2 and (d) SnPc@CeO_2. (II) Methanol yield after repurging CO_2. Reprinted with permission from ref. Kumar, P., A. Kumar, C. Joshi, R. Singh, S. Saran and S.L. Jain. 2015. Heterostructured nanocomposite tin phthalocyanine@mesoporous ceria (SnPc@CeO_2) for photoreduction of CO_2 in visible light. RSC Adv. 5: 42414–42421. Copyright@Royal Society of Chemistry.

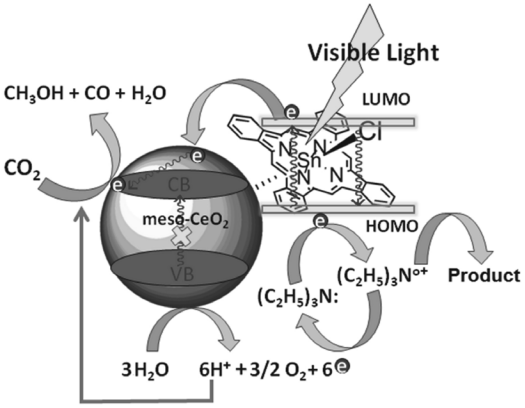

Figure 5. Plausible mechanism of CO_2 reduction over SnPc@CeO_2 catalyst. Reprinted with permission from ref. Kumar, P., A. Kumar, C. Joshi, R. Singh, S. Saran and S.L. Jain. 2015. Heterostructured nanocomposite tin phthalocyanine@ mesoporous ceria (SnPc@CeO_2) for photoreduction of CO_2 in visible light. RSC Adv. 5: 42414–42421. Copyright@Royal Society of Chemistry.

Kumar et al. (2015b) developed a core shell structured bimetallic Ru complex and cobalt phthalocyanine attached TiO_2@SiO_2@Fe_3O_4 microspheres (Ru-CoPc@TiO_2@SiO_2@Fe_3O_4) by step wise coating of SiO_2, TiO_2, CoPc and Ru complex on Fe_3O_4 nanoparticles (Kumar et al. 2015b). The synthesized photocatalyst was found to be much more photoactive in comparison to any component and gave 2570 μmol g^{-1} cat after 48 hr by using water/triethylamine mixture under visible light irradiation. The photocatalyst was magnetically separable and could be reused several times without loss of photoactivity and no leaching of active metallic components such as Ru and Co was observed due to covalent attachment. The particular arrangement was chosen because Ru complex has short life time in comparison to CoPc, so it can transfer

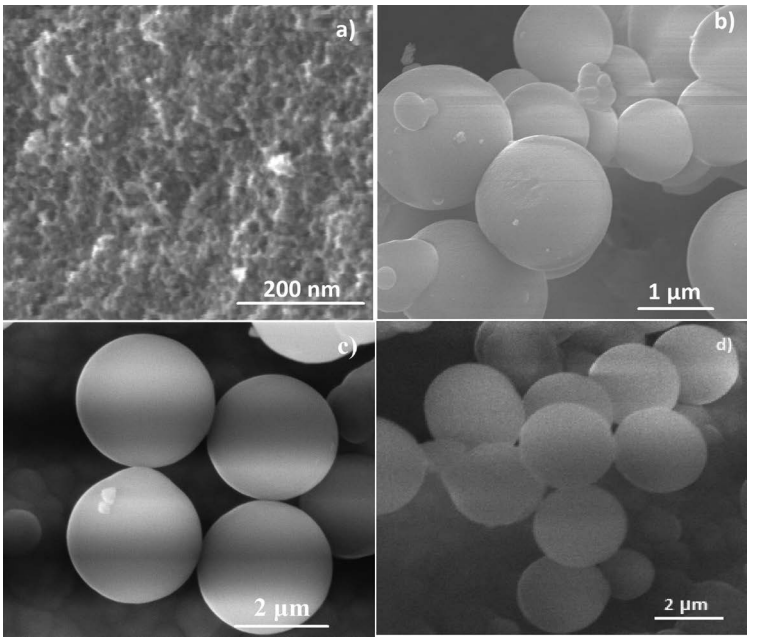

Figure 6. FESEM images of (a) Fe_3O_4, (b) SiO_2@Fe_3O_4, (c) TiO_2@SiO_2@Fe_3O_4, (d) Ru-CoPc@TiO_2@SiO_2@Fe_3O_4. Reprinted with permission from ref. Kumar, P., R.K. Chauhan, B. Sain and S.L. Jain. 2015. Photo-induced reduction of CO_2 using a magnetically separable Ru-CoPc@TiO_2@SiO_2@Fe_3O_4 catalyst under visible light irradiation. Dalton Trans. 44: 4546–4553. Copyright@Royal Society of Chemistry.

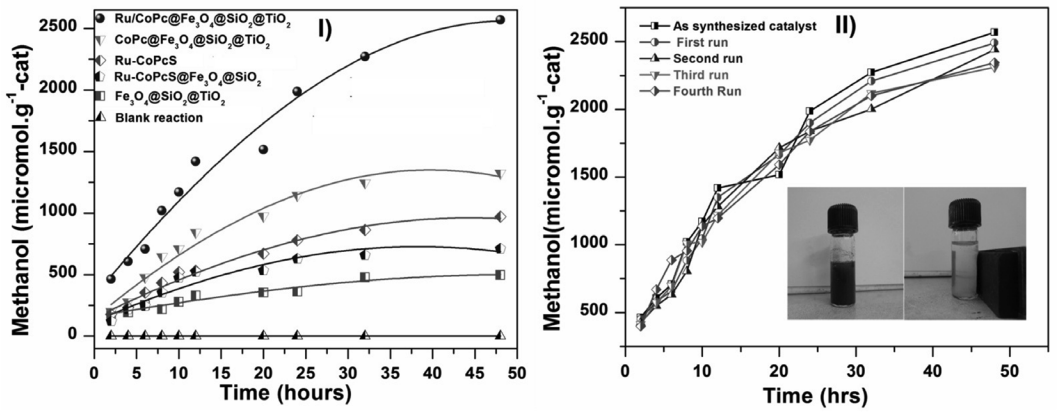

Figure 7. (I) Methanol yield using (a) Ru/CoPc@TiO_2@SiO_2@Fe_3O_4, (b) CoPc@TiO_2@SiO_2@Fe_3O_4, (c) Ru-CoPcS, (d) Ru-CoPcS@SiO_2@Fe_3O_4, (e) TiO_2@SiO_2@Fe_3O_4 and (f) blank run. (II) Recycling of the catalyst. Inset: Magnetic separation of the catalyst using an external magnetic. Reprinted with permission from ref. Kumar, P., R.K. Chauhan, B. Sain and S.L. Jain. 2015. Photo-induced reduction of CO_2 using a magnetically separable Ru-CoPc@TiO_2@SiO_2@Fe_3O_4 catalyst under visible light irradiation. Dalton Trans. 44: 4546–4553. Copyright@Royal Society of Chemistry.

electrons to CoPc faster which has higher life time, so it can efficiently transfer electrons to conduction band of TiO_2. SiO_2 was coated in between TiO_2 and Fe_3O_4 to provide plenty of –OH functionalities for the better coating of TiO_2. Further, it prevents recombination of electrons and protons at Fe_3O_4 core.

In some instances of post grafting approach of immobilization of metal complexes to semiconductors, auto degradation of metal complexes in the presence of light is observed. Thus, to overcome such limitations, *in situ* synthesis of metal complexes grafted semiconductor is a fascinating approach to prevent the loss of metal complex from catalyst support as well as from self degradation. In this regard, Zhao et al. (2009) have synthesized CoPc grafted TiO_2 (CoPc/TiO_2) and elaborate on the reduction of CO_2 to methanol and formic acid. The CoPc/TiO_2 photocatalyst containing 0.7% of CoPc afforded 9.38 mole g cat^{-1} h^{-1} of methanol and 148.81 mole g cat^{-1} h^{-1} of formic acid (Zhao et al. 2009). Kumar and co-workers (2015c) synthesized *in situ* $Ru(bpy)_3Cl_2$ complex grafted TiO_2 (*in situ* $Ru(bpy)_3/TiO_2$) by precipitation of $TiCl_4$ in triethanolamine containing solution followed by dissolution in water and then re-precipitation with ammonia solution (Kumar et al. 2015c). TEM analysis showed fringes of TiO_2 crystal lattice with 0.35 nm (101 plane) interplaner distance that confirmed anatase form (Figure 8-I). Further, wide scan XPS spectra in Ti2p region illustrated characteristics of $Ti2p_{1/2}$ and $Ti2p_{3/2}$ peaks at 464.23 and 458.39 eV binding energy (Figure 8-II). The synthesized *in situ* $Ru(bpy)_3/TiO_2$ photocatalyst was found to be an efficient CO_2 photoreduction catalyst in comparison to TiO_2 synthesized by following same procedure without metal complex. Methanol was identified as the selective reduction product of CO_2 and the obtained formation rate (R_{MeOH}) of methanol was found to be 78.1 μmol g^{-1} h^{-1} after 24 hr under visible light irradiation in the presence of triethylamine as sacrificial donor. The apparent quantum yield (AQY) at 450 nm was calculated to be 0.26 mol $Einstein^{-1}$. Better electron injection to the conduction band of TiO_2 was assumed to be responsible for enhanced photocatalytic performance.

Graphene based materials for solar fuel

A single layer of graphite called graphene has attracted wide attention of scientific community since its discovery by Novoselov et al. (2004). In gaphene, a 2D network of sp^2 hybridized carbon atoms make long range order conjugation which provides exceptional properties like high electron conductivity, thermal conductivity, mechanical strength, optical properties and very high surface area (see Rao et al. 2009, Chen et al. 2012, Hu et al. 2010). Due to these specific properties, graphene has been utilized in

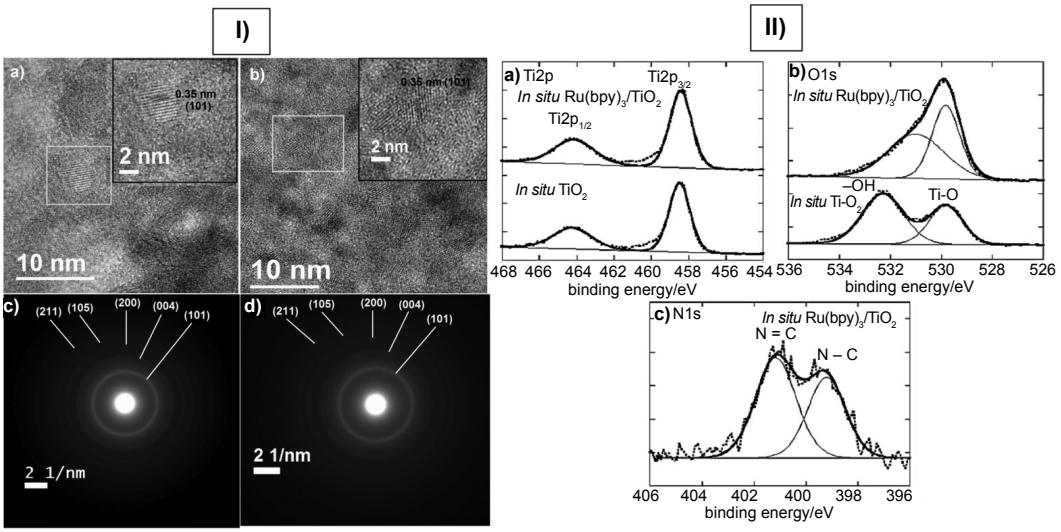

Figure 8. (I) HR-TEM images of (a) *in situ* TiO_2, (b) $Ru(bpy)_3/TiO_2$, SAED patterns of (c) *in situ* TiO_2 and (d) *in situ* $Ru(bpy)_3/TiO_2$. (II) Wide scan XPS spectra of *in situ* TiO_2 and $Ru(bpy)_3/TiO_2$, (a) Ti 2p, (b) O 1s and (c) N 1s region. Reprinted with permission from ref. Kumar, P., C. Joshi, N. Labhsetwar, R. Boukherroub and S.L. Jain. 2015. A novel Ru/TiO_2 hybrid nanocomposite catalyzed photoreduction of CO_2 to methanol under visible light. Nanoscale 7: 15258–15267. Copyright@Royal Society of Chemistry.

various applications like electronic devices, solar energy conversion, super capacitors, sensors, catalysis and particularly for the preparation of composite materials (see Ji et al. 2012, Zhuang et al. 2014, Bai and Shen 2012, Hou et al. 2012, Sahoo et al. 2012). Graphene sheets, due to high mobility of electron on its surface, have been used for the synthesis of nano-hybrid with various semiconductors like TiO_2, ZnO, and Cu_2O nanostructure semiconductors (see Zhang et al. 2012, Cowan and Durrant 2013, Li et al. 2013b, Low et al. 2015).

Ong et al. (2014) used exposed 001 facet anatase doped with nitrogen-doped TiO_2 (N–TiO_2-001) for hybridization with graphene sheets (N–TiO_2-001/GR). The photocatalyst was synthesized by hydrothermal method in one-step using NH_4F as the structure determining agents. In previous studies, it has been showed that 001 facet TiO_2 is more active toward CO_2 reduction. The photocatalytic results showed that N–TiO_2-001/GR nanostructure catalyst gave CH_4 selectively with a yield of 3.70 μmol g^{-1} cat that was 11-fold higher than the TiO_2-001. The enhanced activity was assumed due to three facts: (i) 001 facet TiO_2, (ii) nitrogen doping which reduce band gap, (iii) blending with graphene sheets which provide higher mobility to electrons (Ong et al. 2014).

Harsh oxidation of graphite with strong oxidizing agents like $KMnO_4$ and H_2SO_4 or H_3PO_4 and H_2SO_4 gave graphene oxide, an oxidized form of graphene (see Hummers and Offeman 1958). During the harsh oxidation of graphene, some of the sp^2 carbons get converted into sp^3 hybridized carbons. Thus, enormous sp^2 and sp^3 hybridized domains get evolved on the surface of graphene sheets. The domains having sp^3 carbons due to the presence of tightly held electrons work as valance band while sp^2 domain, due to the presence of mobile electrons, works as conduction band. So oxidation of graphene oxide convert conductive graphene sheets to semiconductor sheets (see Loh et al. 2010, Bonaccorso et al. 2010, Eda et al. 2009). The charge separation phenomenon can take place on the surface of graphene oxide which can be used for the reduction of CO_2 and oxidation of water. In a study, Hsu et al. (2013) has showed that graphene oxide synthesized by $KMnO_4$ and H_2SO_4 using H_3PO_4 as mild oxidizing agent has low band gap 2.9 eV. The synthesized graphene oxide was used for the reduction of CO_2 to methanol under visible light irradiation of xenon lamp as a source of light. The rate of methanol formation was found to be 0.172 μmol g^{-1} cat h^{-1} after 4 hr of visible irradiation that was six-fold higher than pure TiO_2 (see Hsu et al. 2013). The position of conduction band was negative enough (–0.79 V vs. NHE) to facilitate CO_2 reduction to methanol while the position of the valence band (+2.91 V vs. NHE) was positive enough to perform water splitting.

Yeh et al. (2010) have explored the use of graphene oxide for the reduction of protons to hydrogen under visible light irradiation (Yeh et al. 2010). As graphene oxide works as semiconductor, so the phenomenon of charge recombination still exists and so the electron or hole capturing agents can improve the photocatalytic performance. So, addition of platinum nanoparticles as electron capturing agents and methanol as hole scavenger improve the yield of hydrogen from 280 μmol after 6 hr for GO to 17000 μmol after 6 hr for Pt/GO having methanol as hole scavenger. In another study by Shown et al. (2014), copper nanoparticles (4–5 nm) modified GO (10 wt% Cu-NPs) has been found to increase the rate of methanol production from 0.172 μmol g^{-1} cat h^{-1} after 4 hr to 2.94 μmol g^{-1} h^{-1} after 2 hr with acetaldehyde as byproduct (3.88 μmol g^{-1} h^{-1}) (Shown et al. 2014). The increased yield was assumed due to capturing of electrons which lower the electron hole pair recombination.

Nanostructured composite of graphene oxide with various semiconductor materials exhibits higher photocatalytic performance because of transfer of electrons from semiconductors to GO which can move apart on the surface. High specific surface area provides better adsorption of CO_2 and H_2O molecule. Further modified semiconductors have narrow band gap and can induce charge production at higher wave length. In this regard, Tan et al. (2015a) synthesized a composite of oxygen rich TiO_2 and graphene oxide (GO-OTiO_2) for CO_2 reduction. The oxygen rich TiO_2 was prepared by precipitation of titanium butoxide in the presence of hydrogen peroxide (Tan et al. 2015a). Due to the narrowing of band gap and creation of defects, the TiO_2 was visible light active with a band gap of 2.95 eV. The optimal loading of GO which promotes better CO_2 reduction was calculated to be 5 wt%. After 6 hr of visible irradiation, the yield of CH_4 over GO-TiO_2 nanocomposite was found to be 1.718 μmol g^{-1} cat which was 14 times higher than commercial grade P25 TiO_2.

Due to rich surface chemistry, graphene oxide also serves as semiconductor support for attachment of various semiconductors and metal complexes. Graphene oxide has absorption range in 230 to 300 nm, so it can absorb light of lower wave length. Hybridization with metal complex further improves the visible light absorption profile along with the significant enhancement in CO_2 conversion efficiency. Kumar et al. (2015d) have immobilized a ruthenium heteroleptic complex to GO by using chloroacetic acid as linker (Kumar et al. 2015d). The developed photocatalyst showed increased yield of methanol in comparison to graphene oxide alone. The methanol formation rate and quantum yield at 510 nm for GO-Ru catalyst was found to be 85.4 μmol g^{-1} cat h^{-1} after 24 hr and (ϕ_{MeOH}) of 0.09, respectively, while for GO alone this value was 20.0 μmol g^{-1} cat h^{-1} and 0.044, respectively. The increased conversion efficiency was assumed due to continuous pumping of electrons from excited ruthenium complex to conduction band of GO. In a similar approach, CoPc was also used as anchoring photosensitizer unit because of its wide absorption pattern in visible region and longer life time of excited state (see Kumar et al. 2014a). Ruthenium trinuclear complex, which works as antenna and collects photogenerated electrons, was also immobilized to GO for photocatalytic CO_2 activation to methanol (see Kumar et al. 2014b). It can transfer multiple electrons so it creates possibility for getting higher hydrocarbons. The synthesized photocatalyst was used for the photocatalytic reduction of CO_2 to methanol using triethylamine as a reductive quencher by using 20 W LED as visible light source. The yield of methanol was found to be 3977.57 ± 5.60 μmol g^{-1} cat after 48 hr.

Reduced graphene oxide as obtained by reduction of graphene oxide is also well documented for the photocatalytic applications. In this regard, Tan and co-workers (2013) synthesized reduced graphene oxide TiO_2 (rGO-TiO_2) nano-hybrid by solvothermal method and obtained CH_4 product in 0.135 μmol $g_{cat}^{-1} h^{-1}$ yield after 4 hr of reaction (Tan et al. 2013). Composite of Cu_2O semiconductor with reduced graphene oxide (Cu_2O/RGO) posseses higher photocatalytic performance for reduction of CO_2. Addition of 0.5% RGO was found to be of the optimal amount and the Cu_2O/0.5% RGO composites produce CO at an average of 50 ppm $g^{-1} h^{-1}$ after 20 h, with an apparent quantum yield of 0.34% at 400 nm. This yield was approximately 50 times higher than bare Cu_2O which clearly explains the role of graphene oxide as charge separator (see An et al. 2014). During the reduction step of graphene oxide, oxygen carrying moieties are removed which create defects in graphene sheets and diminish charge mobility over the sheets. In a study, Liang et al. showed that the solvent exfoliated graphene (SEG) synthesized by ultrasonication in *N,N*-dimethyl formamide (DMF) has less defect in comparison to rGO synthesized with chemical reduction methods, which improves electrons' mobility on the sheets. A composite of SEG with TiO_2 (P-25) SEG (0.27%)-TiO_2 synthesized by using ethyl cellulose as a stabilizing and film forming polymer can reduce CO_2 to methane with a formation rate of 8.3 μmol $h^{-1} m^{-2}$ under UV light irradiation that was 4.5 times higher than bare TiO_2 (see Liang et al. 2011). Yu et al. (2014) reported that reduced graphene (RGO)–CdS nanorod composite prepared by a one-step microwave-hydrothermal method in an ethanolamine–water solution exhibited a higher activity for the photocatalytic reduction of CO_2 to CH_4, without any co-catalyst (Yu et al. 2014b).

Noble metals like Pt, Pd, Ag and Au nanoparticles decorated on reduced graphene oxide/TiO_2 (GT) were also tested for photoreduction of CO_2 to explore the better charge capturing performance of noble metals in composite. Among the noble metals used, the Pt-doped GT nanocomposites were found to be the most active and afforded CH_4 yield up to 1.70 μmol g^{-1} cat after 6 hr of light irradiation, that was 2.6 and 13.2 folds higher in comparison to GT and commercial P25, respectively (see Tan et al. 2015b).

In a recent report by Gusain et al. (2016), reduced graphene oxide (rGO)–copper oxide (rGO-CuO) nanocomposites were prepared by grafting of CuO nanorods on the rGO sheets (Gusain et al. 2016). Surface modification of CuO naorods by APTMS (3-aminopropyl-trimethoxysilane) led to accumulation of positive charge which interacts with negatively charged graphene oxide sheets. These GO modified CuO nanorods after hydrothermal treatment produce rGO-CuO nanocomposite. The NaOH to copper salt ratio determines the width of CuO nanorods in composite. By using different NaOH:$(CH_3COOH)_2Cu$ ratio, the thickness of CuO nanorods in rGO-CuO nanocomposite was found to be 3–6, 5–9, 9–11 and 10–15 nm for rGO-CuO_{14}, rGO-CuO_{18}, rGO-CuO_{116} and rGO-CuO_{124} nanocomposites, respectively (Figure 9-I). High resolution XPS spectra in Cu2p region gave an intense peak at ~933.5 eV with associated satellite peaks for Cu^{+2} state confirming the presence of CuO in composite (Figure 9-II). Methanol was

obtained selectively in CO_2 photoreduction experiment and rGO-CuO_{116} composite gave the highest yield of methanol with a formation rate (R_{MeOH}) of 51.1 μmol g^{-1} h^{-1} after 24 h. Recycling experiments showed that the synthesized photocatalyst was stable and recyclable for several runs without compromising the performance of catalyst (Figure 9-III). The increased performance was explained due to higher mobility of electrons on rGO sheets, which prevents electron and hole recombination (Figure 10).

Making composite of graphene not only improves charge separation on its surface but also, in some cases it has been observed that graphene can raise the position of conduction band of semiconductor. A

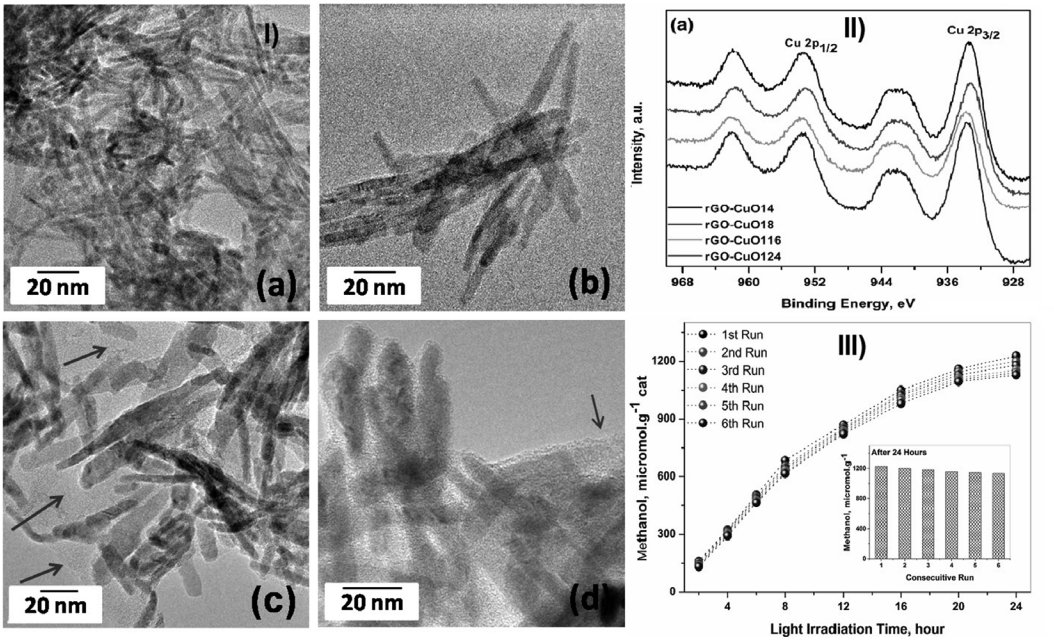

Figure 9. (I) HRTEM images of (a) rGO–CuO14, (b) rGO–CuO18, (c) rGO–CuO116 and (d) rGO–CuO124 nanocomposites. (II) High resolution XPS in Cu 2p region of rGO–CuO14, rGO–CuO18, rGO–CuO116 and rGO–CuO124 nanocomposites. (III) Recycling results by using rGO–CuO116 photocatalyst for the methanol yield as a function of irradiation time. Reprinted with permission from ref. Gusain, R., P. Kumar, O.P. Sharma, S.L. Jain and O.P. Khatri. 2016. Reduced graphene oxide–CuO nanocomposites for photocatalytic conversion of CO_2 into methanol under visible light irradiation. Appl. Catal. B 181: 352–362. Copyright@Elsevier.

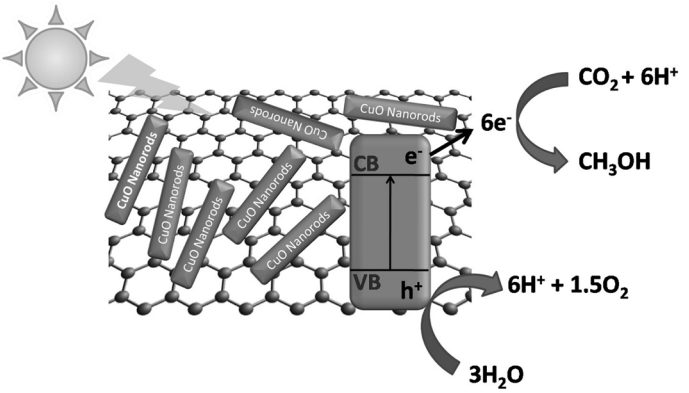

Figure 10. Schematic illustration of photocatalytic conversion of CO_2 to methanol, by using rGO–CuO nanocomposites under visible light irradiation. Reprinted with permission from ref. Gusain, R., P. Kumar, O.P. Sharma, S.L. Jain and O.P. Khatri. 2016. Reduced graphene oxide–CuO nanocomposites for photocatalytic conversion of CO_2 into methanol under visible light irradiation. Appl. Catal. B 181: 352–362. Copyright@Elsevier.

recent report by Wang et al. 2013b showed that blending of graphene with WO_3 raises the position of conduction band which makes it more reductive for the efficient reduction of CO_2. The CB band edge value of WO_3 was found to be –0.10 V vs. NHE at pH-7 which was low for the reduction of CO_2, while for WO_3/rGO composite the conduction band edge position was found to be –0.47 V (obtained by XPS VB spectra) which was negative enough to promote CO_2 reduction to methane. After 8 hours of visible irradiation, the yield of CH_4 was found to be 0.89 μmol g^{-1} cat.

Doping of heteroatoms such as N, S, B, P, etc. to graphene oxide is a well known approach to enhance its photocatalytic activity (see Lin et al. 2012). Nitrogen doping removes carbon atoms from the surface of graphene and three types of nitrogen pyridinic, quarternary nitrogen, and pyrrolic were evolved depending upon their position on the sheets. The contribution of electron pair by pyridinic nitrogen in π conjugated network of graphene transforms sheets in electron rich sheets and Fermi level shift above the Dirac point which distorts the symmetry of graphene sub lattice and creates a band gap. The band gap of N-doped graphene is highly dependent on the nitrogen content and a band gap value up to 5 eV can be reached. Nitrogen doping can be achieved by either *in situ* synthesis in the presence of nitrogen containing substrate or via post grafting approach using gaseous nitrogen source. Nitrogen doping disturbs the charge distribution on neighbouring atoms and negative charge gets accumulated on the surface of graphene which creates "activation region" on the graphene sheets. Due to the presence of these activation regions, N-doped graphene can be used for various reactions and attachment of metal particles/semiconductors/ metal complexes, etc. The nanostructured composite of N-doped graphene with various semiconductor materials has been proven to show superior photocatalytic performance. Reduction of graphene oxide in the presence of phosphorous source like phosphoric acid, P-containing ionic liquids, etc. produce P-doped graphene. Phosphorous atoms due to loosely held electrons on the sheets make sheets more electron rich in character and afford higher band gap in comparison to N-doped graphene which can be used for the proton or CO_2 reduction. Sanchez et al. synthesized P-doped graphene (P)G-4 by pyrolysis of $H_2PO_4^-$ modified alginate at 900ºC under inert atmosphere and were able to tune band gap up to 2.85 eV. Further, phosphorous content was calculated with the help of XPS which reveal 12.73% phosphorous. The catalyst was able to produce hydrogen from water in the presence triethanolamine as sacrificial donor. Furthermore, immobilization of metal complexes to N-doped graphene for photoreduction of CO_2 to methanol is also documented in the literature. In this regard, Kumar et al. (2015e) reported copper complex $[Cu(bpy)_2(H_2O)_2]Cl_2.2H_2O$ supported on N-doped graphene (GrN_{700}-CuC) as efficient photocatalyst for photoreduction of CO_2 into CH_3OH with a conversion rate of 0.77 μmol g^{-1} h^{-1} with the associated quantum yield of 5.8 x 10^{-4} after 24 hr under visible light irradiation. The nitrogen content of N-doped graphene was found to be 6.01% which was enough to create a band gap required for the reduction of CO_2 (Kumar et al. 2015e).

A nanocomposite of boron doped graphene and P25 TiO_2 (P25/B-GR) was used for the reduction of CO_2 to methane (see Xing et al. 2014). Boric acid (H_3BO_3) was used as a source of boron for the synthesis of B-doped graphene. It has been well documented in literature that exposure of ZZ-edges on nanoscaled graphene give rise to semi-metallic property. B-doping in graphene has many exposed ZZ-edges and thus, the photo-generated electrons of B-GR make its Fermi level (E'_f-B-GR nanosheets) higher than the conduction band (EC-GR sheets) of GR sheets (from E_f-B-GR nanosheets to E'_f-B-GR nanosheets). The Fermi level of B-doped graphene lies in between the conduction band of TiO_2 and reduction potentials of CO_2/CH_4, so electrons can be transferred from CB of TiO_2 to B-doped nanosheets. The as prepared composite after 120 min solar light irradiation showed the highest photo generation of CH_4 (> 2.50 μmol g^{-1}).

Photocatalysis by metal clusters based nanostructured composite

Metal clusters, a class of Polyoxometalates (POMs), are molecular metal oxide aggregates and are typically formed by oligo-condensation reactions of small oxometalate precursors, often in the presence of templating anions (see Kibsgaard et al. 2014). Octahedral metal clusters of Mo and Re can be good photocatalyst for various applications including CO_2 reduction and hydrogen evolution. These are an attractive alternative because of the presence of multi-metallic centres that can transfer multiple electrons

to reduce CO_2 to give higher hydrocarbons. Metal clusters are fully oxidized with d_0 configuration and show LMCT (ligand to metal charge transfer) transition in the range of 200–500 nm due to O→M transition. Recently, work group of Hill et al. (2012) reported cobalt based Polyoxometalates (POMs, clusters) as photocatalysts for the solar water splitting. Further, $[Ru(bpy)_3]^{2+/3+}$ redox photosensitizer modified cobalt-POM-cluster $[CoII_4(H_2O)_2(PW_9O_{34})_2]^{10-}$ was found to be good photocatalyst for water oxidation (Zhu et al. 2012). The photosensitizer unit acts as electron shuttle that transfers electrons to water-oxidising Co-POM cluster. A work by Kumar et al. (2014c) used octahedral molybdenum $[Mo_6Br_{14}]^{2-}$ having Cs^+ and TBA^+ (tetrabutylammonium) counter ions as CO_2 reduction catalyst with higher quantum efficiency (Kumar et al. 2014c). However, due to their homogeneous nature, they are difficult to recover and recycle. Thus, to overcome these drawbacks metal clusters have been immobilized to photoactive semiconductor supports. Fabre et al. (Fabre et al. 2014, Cordier et al. 2010) immobilized octahedral cluster on n-type and p-type Si (111) surface modified with pyridine terminated alkyl layer by taking advantage of labile nature of apical halogen atoms (Fabre et al. 2009, Cordier et al. 2010). Graphene oxide, due to presence of plenty oxygenated groups, has been identified as suitable supporting material. Kumar et al. (2015f) have immobilized octahedral Mo clusters on GO by replacement of apical bromine atoms by oxygen carrying functionalities present on the surface of graphene oxide (Kumar et al. 2015f). Methanol was observed as the sole CO_2 reduction product by using GO-$Cs_2Mo_6Br^i_8Br^a_x$ (i = icosahedral, a = apical) and GO-$(TBA)_2Mo_6Br^i_8Br^a_x$ as photocatalysts and the formation rate was found to be 68.5 and 53.9 μmol g^{-1} h^{-1}, respectively, after 24 hr irradiation under visible light without using any sacrificial donor. The obtained quantum yield and turn over number by using GO-$Cs_2Mo_6Br^i_8Br^a_x$ was calculated to be 0.015 and 19.0 respectively, while for GO-$(TBA)_2Mo_6Br^i_8Br^a_x$ these values were 0.011 and 10.38, respectively. The plausible mechanism defines that metal clusters after absorption of visible light get excited and transfer electrons and positive charge to CB and VB of GO, respectively, so indirectly charge pairs get evolved on GO that was used for CO_2 reduction and water oxidation.

In a study, Kumar et al. (2015g) synthesized octahedral hexacyano rhenium $K_4[Re_6S_8(CN)_6]$ cluster complexes which were grafted onto photoactive $Cu(OH)_2$ cluster modified TiO_2 {$Cu(OH)_2/TiO_2$} support (Kumar et al. 2015g). In a previous report, $Cu(OH)_2$ cluster modified TiO_2 has been identified as good hydrogen evolving catalyst (see Yu and Ran 2011), so it was used as an active support for the immobilization of Re clusters. Re cluster molecules were immobilized covalently by Re-CN-M bridges bond formation. The methanol yield after 24 hr irradiation was found to be 149 μmol/0.1 g cat for Re-cluster@$Cu(OH)_2/TiO_2$ photocatalyst that is much higher than 35 μmol/0.1 g cat for $Cu(OH)_2/TiO_2$ and 75 μmol/0.1 g cat for equimolar rhenium cluster in the presence of triethanolamine (TEOA) as a sacrificial donor. The quantum yields (ϕ_{MeOH}) of Re-cluster@$Cu(OH)_2/TiO_2$ and $Cu(OH)_2/TiO_2$ were

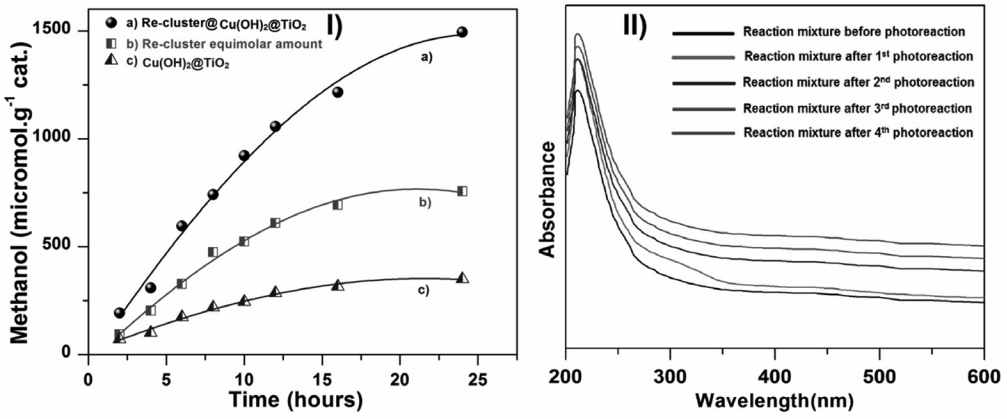

Figure 11. (I) CO_2 conversion to methanol using (a) Re-cluster@$Cu(OH)_2/TiO_2$, (b) Re complex at same equimolar amount and (c) $Cu(OH)_2/TiO_2$. (II) UV–vis spectra of reaction mixtures of recycling experiments. Reprinted with permission from ref. Kumar, P., N.G. Naumov, R. Boukherroub and S.L. Jain. 2015. Octahedral rhenium $K_4[Re_6S_8(CN)_6]$ and $Cu(OH)_2$ cluster modified TiO_2 for the photoreduction of CO_2 under visible light irradiation. Appl. Catal. A 499: 32–38. Copyright@Elsevier.

found to be 0.018 and 0.004 mol Einstein^{-1}, respectively (Figure 11-I). The catalyst was recyclable and no loss in activity was observed. Further, after every recycling, the UV-Vis spectra of solution was measured which showed no leaching of cluster from the surface of modified $Cu(OH)_2/TiO_2$ semiconductor support (Figure 11-II).

The $Cu(OH)_2$ clusters modified TiO_2 has band gap 3.11 eV which was somewhat lower than TiO_2. The reduction potential of $Cu(OH)_2/Cu$ is −0.634 V (vs. NHE at pH-7), which was negative enough for the reduction of CO_2 to methanol {CO_2/CH_3OH (−0.38 V vs. NHE at pH-7)} and H^+/H_2(−0.41 V vs. NHE at pH-7). So electrons can be transferred from TiO_2 CB to $Cu(OH)_2$ and, subsequently, to CO_2 or proton.

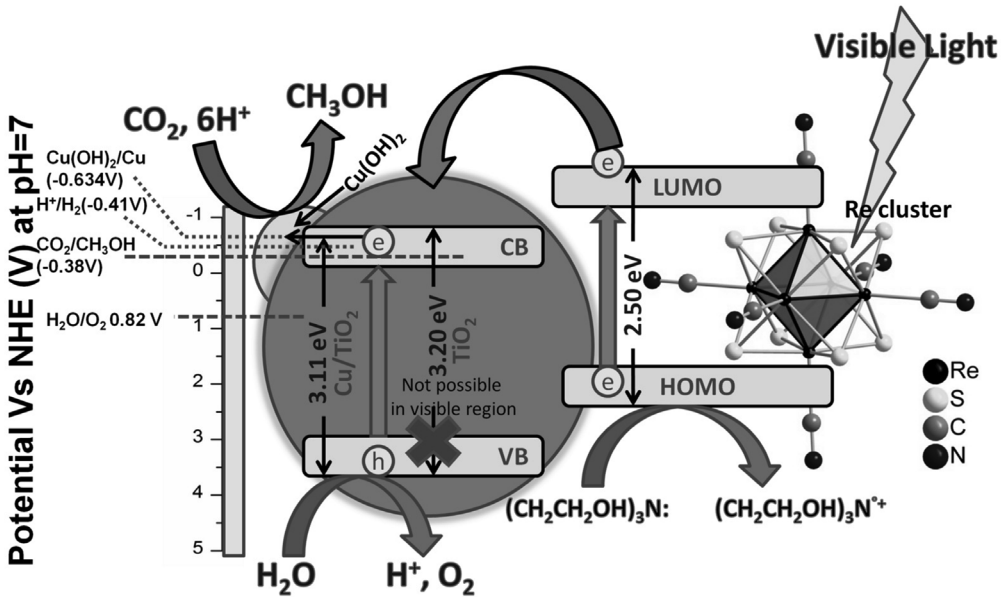

Figure 12. Plausible mechanism of CO_2 reduction by Re-cluster@$Cu(OH)_2/TiO_2$ under visible light irradiation. Reprinted with permission from ref. Kumar, P., N.G. Naumov, R. Boukherroub and S.L. Jain. 2015. Octahedral rhenium $K_4[Re_6S_8(CN)_6]$ and $Cu(OH)_2$ cluster modified TiO_2 for the photoreduction of CO_2 under visible light irradiation. Appl. Catal. A 499: 32–38. Copyright@Elsevier.

However, the value of reduction potential of CO_2 is more negative than reduction potential of proton, so CO_2 reduction win over proton reduction and methanol was observed as a major reaction product (Figure 12).

Graphitic carbon nitride as photocatalyst

Semiconductor polymeric materials have gained considerable importance in recent years due to their flexibility for structure modification and tuning of band gap by degree of polymerization. Among various polymeric materials known, graphitic carbon nitride is important due to its low band gap (2.7 eV) and suitable position of conduction band (–1.1 eV) and valence band (+1.6 eV) (see Ong et al. 2016). Carbon nitride is a 2D polymer consisting of interconnected tri-s-triazines units via tertiary amines. Carbon nitride is mainly synthesized with dicyanamide, melamine, etc. For example, Wang et al. (2009b) synthesized carbon nitride by heating melamine in air and used it for photocatalytic water splitting (Wang et al. 2009b). However, the precursor melamine is expensive, difficult to obtain and highly explosive, so urea can be used as a cost effective and non-toxic alternative for preparation of carbon nitride. Dong and coworkers (2012) synthesized a layered g-C_3N_4 with a high surface area by directly heat treating the urea in air, which exhibited much higher visible light photoactivity (Dong et al. 2012). The band gap can be further reduced via doping with heteroatoms like P, S and I, etc. (see Zhang et al. 2014). Recently, Zhang

et al. (2010) synthesized P-doped g-C_3N_4 by using 1-butyl-3-methylimidazolium hexafluorophosphate ($BmimPF_6$) as a source of phosphorous and obtained an improved photocurrent response (Zhang et al. 2010). Hong et al. (2012) prepared S-doped mesoporous carbon nitride (mpgCNS) by *in situ* method and observed higher hydrogen evolution rate in comparison to mpgCN (Hong et al. 2012).

As carbon nitride possesses graphene like sheets for better mobility to electrons and small band gap, therefore, it has been combined with other semiconductor materials like $BiVO_4$, TaON, $BiPO_4$, TiO_2, WO_3, $NaNbO_3$, Cu_2O, Bi_2WO_6, to obtain nano-hybrids for various applications including hydrogen evolution and CO_2 reduction. Porosity is the main feature which determines the concentration of reactant on the photocatalyst surface and therefore the photocatalytic performance (see Xu et al. 2013c, Portehault et al. 2010, Yan et al. 2010, Pan et al. 2012, Ge et al. 2011).

Kailasam et al. (2011) synthesized highly mesoporous carbon nitride by sol gel method using silica as template. Ordered structured mesoporous carbon nitride was prepared by facile sol-gel route using precursor TEOS as source of silica and cyanamide as the source for carbon nitride. The synthesized porous carbon nitride was used for solar hydrogen evolution experiment and it has been found that sample CN-6 (1:6, TEOS:CN) gave the highest yield of hydrogen (40.5 H_2/mL) after 24 h using K_2PtCl_6 as catalyst and TEOA as sacrificial donor (Kailasam et al. 2011).

In another report, Kailasam et al. (2015) synthesized WO_3/carbon nitride (W-TEOS-CN) composite by simple mixing of precursor cyanamide, TEOS, followed by addition of WO_3 (Kailasam et al. 2015). The synthesized composite was found to be very active for hydrogen evolution and the rate of hydrogen evolution could be reached up to 326 μmol H_2 h^{-1}, which was 2.4 times of simple nanoporous carbon nitride. The enhanced activity was assumed due to the efficient charge separation via Z-scheme and this was confirmed by photoluminescence (PL) spectroscopic analysis.

Shi and co-workers (2014) synthesized visible-light-responsive g-C_3N_4/$NaNbO_3$ nanowires by fabrication of polymeric g-C_3N_4 on $NaNbO_3$ nanowires. The calculated value of optical band gap for $NaNbO_3$ and g-C_3N_4 was found to be 3.4 and 2.7 eV, respectively, so the addition of g-C_3N_4 generates heterojunction which facilitates electron transfer from carbon nitride to $NaNbO_3$. During the first 4 hr of irradiation, the rate of CH_4 generation over Pt-g-C_3N_4/$NaNbO_3$ was as high as 6.4 μmol h^{-1} g^{-1} in contrast to that of Pt-g-C_3N_4 (0.8 μmol h^{-1} g^{-1}) (Shi et al. 2014).

As can be seen in the existing literature, most of semiconductor photocatalysts use expensive noble metals like Pt, Pd, Ru, Ir, etc. as charge capturing species. These noble metals can activate substrate molecules by bond formation which further facilitates CO_2 reduction/protons reduction. However, the addition of noble metal adds extra cost which makes the process less viable from economical viewpoints. So, efforts are directed for designing photocatalyst which can work without noble metal dopants. The core shell $LaPO_4$/g-C_3N_4 nanowires synthesized via an *in situ* hydrothermal growth of $LaPO_4$ nanorods in tubular g-C_3N_4 was investigated for photocatalytic conversion of CO_2 to CO in the absence of any noble metal (see Li et al. 2017). The irradiation of 30 mg nanocomposite yielded 0.433 μmol of CO from CO_2 within 1 hr irradiation. Photoluminescence spectra (PL spectra) of $LaPO_4$ showed the lowest PL intensity due to the small amount of charge generation. The g-C_3N_4 showed the highest PL intensity because of charge generation under visible light. However, core shell structure formation by on $LaPO_4$ quenched PL signal which was probably due to charge transfer from g-C_3N_4 to $LaPO_4$ (Li et al. 2017).

The photo-efficiency of carbon nitride material can be further increased by sensitization with metal complexes. Recently, Takanabe et al. (2010) have immobilized magnesium phthalocyanine on carbon nitride by π–π stacking interaction and observed enhanced photocatalytic performance for water splitting (Takanabe et al. 2010). Ruthenium complex (trans(Cl)-[$Ru(bpyX_2)(CO)_2Cl_2$]) immobilized on carbon nitride via phosphate linkers has been found a potent catalyst for photoreduction of CO_2 to CO under visible light (see Kuriki et al. 2015). Graphitic carbon nitride also works as CO_2 capturing agent so it can capture and reduce CO_2 simultaneously. Lin et al. (2014) developed a cobalt bipyridine redox catalyst modified carbon nitride, $Co(bpy)_3^{+2}/C_3N_4$, system, having cobalt oxide and hole capturing agent for photocatalytic reduction of CO_2 to CO under visible light irradiation (Lin et al. 2014). In a work by Kuriki et al. (2016), they have synthesized ruthenium binuclear complex supported on graphitic carbon nitride via phosphate moiety (RuRu'/C_3N_4) for the photoreduction of CO_2 to HCOOH in visible light region (Kuriki et al. 2016). Further, modification of carbon nitride with silver nanoparticles increases

the yield of formic acid (TON > 33,000 with respect to the amount of RuRu'/Ag/C_3N_4). Kumar and co-workers (2016) have synthesized iron bipyridyl complex grafted nanoporous carbon nitride ($Fe(bpy)_3$/npg-C_3N_4) which was used for visible light, mediating the amines oxidative coupling (Kumar et al. 2016).

Other carbonaceous materials for CO_2 activation

Apart from graphene, carbon nitride and other carbonaceous materials like fullerene, carbon nanotube (CNT), carbon quantum dots (CDs), etc. have also been explored for the CO_2 activation applications. For example, Wu et al. (2015) reported nitrogen doped carbon nanotube which due to the presence of pyridinic nitrogen generated electron rich defects that work as active sites for the reduction of CO_2 (Wu et al. 2015). Liang et al. (2012) synthesized a composite of single walled carbon nanotube−titania nanosheet (SWCNT−TiNS) with low carbon defect densities for investigating role of carbon nanomaterial dimensionality on photocatalytic response. However, the photoactivity of SWCNT−TiNS composite for methane production was found to be less than solvent exfoliated graphene-titania nanosheet SEG−TiNS but this activity was much higher than bare titania nanosheet (Liang et al. 2012).

Carbon nanodots, due to the quantum confinement effect, have been emerged as new photocatalytic materials. C Dots have been used for various application, fluorescence emission, dye degradation, energy conversion and storage, etc. (see Fernando et al. 2015). Carbon dots, due to the presence of graphene like oxidized sheets, can work as semiconductor and the optical properties are strongly dependent on their size. Further, like graphene, their band gap can be reduced by doping with nitrogen. A work by Sahu et al. (2014) has synthesized carbon quantum dots decorated with Au nanoparticles for solar light harvesting. Various small hydrocarbon molecules were observed with higher selectivity for formic acid. Interestingly, the increase in CO_2 pressure enhances the yield of products (formic acid and acetic acid were 1.2 and 0.06 mmol h^{-1} g^{-1}), at 700 psi and 405−720 nm wavelength for 4 hr due to better absorption of CO_2 at elevated pressure (Sahu et al. 2014). In a similar study, Choi et al. (2013) prepared Ag decorated carbon dots by decomposition of cyclodextrin under UV light in the presence of $AgNO_3$ (Choi et al. 2013).

Very recently, Yadav et al. (2016) reported 6-amino-2-(9,10-dioxo-6-(2-(perylen-3-yl)-4,5-di-p-tolyl-4,5-dihydro-1H-imidazol-1-yl)-9,10-dihydroanthracen-2-yl)-1Hbenzo[de]isoquinoline-1,3(2H)-dione (ANP) functionalized graphene quantum dots coupled with formate dehydrogenase (FDH) enzyme as potent photocatalyst for selective reduction of CO_2 to formic acid (Yadav et al. 2016).

Conclusion

Various nanostructured composites including semiconductors and carbon materials hybrids have been explored thoroughly for photocatalytic activation of water, carbon dioxide and other molecules. Photocatalytic conversion of CO_2 to solar fuel by means of artificial photosynthesis is a challenging aspect which has the potential to solve both the issues related to global warming as well as depleting energy resources. Thus, the field of development of photocatalytic systems for CO_2 reduction using solar light is likely to be a topic of tremendous importance in the prospects of current situation. CO_2 reduction over unmodified semiconductor material afforded poor yield of photoreduced products due to the large band gap which makes this approach far from realization. However, band gap engineering with doping, mixing with low band gap semiconductor, sensitization with metal complexes or hybridization with various nanomaterials can produce nanohybrid photocatalysts with tuned band edge positions that can sustain CO_2 reduction and water oxidation process. The efficient separation of photogenerated charge is the key for achieving higher conversion efficiency, so electron and hole capturing agents play a pivotal role, and facilitate charge separation. Carbon materials such as graphene oxide, reduced graphene oxide, and carbon nitride have shown to provide enhanced quantum yield due to higher mobility of charge carrier which prevents recombination. Doping with heteroatoms and composite formation with different band gap materials showed higher photocatalytic performance. Among the various known approaches, hybridization of semiconductors with metal complexes seems to be the most promising one to get higher hydrocarbon products in enough concentration to reduce impact of CO_2 concentration on environment.

References

Ahmed, N., Y. Shibata, T. Taniguchi and Y. Izumi. 2011. Photocatalytic conversion of carbon dioxide into methanol using zinc–copper–M (III) (M = aluminum, gallium) layered double hydroxides. J. Catal. 279: 123–135.

Ajayaghosh, A. 2003. Donor–acceptor type low band gap polymers: polysquaraines and related systems. Chem. Soc. Rev. 32: 181–191.

An, X., K. Li and J. Tang. 2014. Cu_2O/reduced graphene oxide composites for the photocatalytic conversion of CO_2. ChemSusChem. 7: 1086–1093.

Aresta, M., A. Dibenedetto and A. Angelini. 2014. Catalysis for the valorization of exhaust carbon: from CO_2 to chemicals, materials, and fuels. Technological use of CO_2. Chem. Rev. 14: 1709–1742.

Atabani, A.E., A.S. Silitonga, I.A. Badruddin, T.M.I. Mahlia, H.H. Masjuki and S. Mekhilef. 2012. A comprehensive review on biodiesel as an alternative energy resource and its characteristics. Renew. Sustain. Energy Rev. 16: 2070–2093.

Bachu, S. 2008. CO_2 storage in geological media: role, means, status and barriers to deployment. Pro. Energy Combus. Sci. 34: 254–273.

Bai, S. and X. Shen. 2012. Graphene–inorganic nanocomposites. RSC Adv. 2: 64–98.

Balcerski, W., S.Y. Ryu and M.R. Hoffmann. 2007. Visible-light photoactivity of nitrogen-doped TiO_2: photo-oxidation of HCO_2H to CO_2 and H_2O. J. Phys. Chem. C 111: 15357–15362.

Barber, J. 2009. Photosynthetic energy conversion: natural and artificial. Chem. Soc. Rev. 38: 185–196.

Barelli, L., G. Bidini, F. Gallorini and S. Servili. 2008. Hydrogen production through sorption-enhanced steam methane reforming and membrane technology: a review. Energy 33: 554–570.

Bonaccorso, F., Z. Sun, T. Hasan and A.C. Ferrari. 2010. Graphene photonics and optoelectronics. Nat. Photonics 4: 611–622.

Brand, B. and K. Blok. 2015. Renewable energy perspectives for the North African electricity systems: a comparative analysis of model-based scenario studies. Energy Strat. Rev. 6: 1–11.

Brownson, D.A.C., D.K. Kampouris and C.E. Banks. 2011. An overview of graphene in energy production and storage applications. J. Power Sources 196: 4873–4885.

Cempbell, J.E., D.B. Lobell, R.C. Genova and C.B. Field. 2008. The global potential of bioenergy on abandoned agriculture lands. Environ. Sci. Tech. 42: 5791–5794.

Chang, Y.H., W. Zhang, Y. Zhu, Y. Han, J. Pu, J.K. Chang et al. 2014. Monolayer $MoSe_2$ grown by chemical vapor deposition for fast photodetection. ACS Nano 8: 8582–8590.

Chen, D., H. Feng and J. Li. 2012. Graphene oxide: preparation, functionalization, and electrochemical applications. Chem. Rev. 112: 6027−6053.

Chestnoy, N., T.D. Harris, R. Hull and L.E. Brus. 1986. Luminescence and photophysics of cadmium sulfide semiconductor clusters: the nature of the emitting electronic state. J. Phys. Chem. 90: 3393–3399.

Choi, H., S.-J. Ko, Y. Choi, P. Joo, T. Kim, B.R. Lee et al. 2013. Versatile surface plasmon resonance of carbon-dot-supported silver nanoparticles in polymer optoelectronic devices. Nat. Photonics 7: 732–738.

Choudhary, S., S. Upadhyay, P. Kumar, N. Singh, V.R. Satsangi, R. Shrivastav et al. 2012. Nanostructured bilayered thin films in photoelectrochemical water splitting—A review. Int. J. Hydro. Energy 37: 18713–18730.

Chouhan, N., R.S. Liu and S.F. Hu. 2013. Cd-ZnGeON solid solution: the effect of local electronic environment on the photocatalytic water cleavage ability. J. Mater. Chem. A 1: 7422–7432.

Cook, T.R., D.K. Dogutan, S.Y. Reece, Y. Surendranath, T.S. Teets and D.G. Nocera. 2010. Solar energy supply and storage for the legacy and nonlegacy worlds. Chem. Rev. 110: 6474–6502.

Cordier, S., B. Fabre, Y. Molard, A.-B.F.-Djomkam, N. Tournerie, A. Ledneva et al. 2010. Covalent anchoring of Re6Sei8 cluster cores monolayers on modified n-and p-type Si (111) surfaces: Effect of coverage on electronic properties. J. Phys. Chem. C 114*:* 18622–18633.

Cowan, A.J. and J.R. Durrant. 2013. Long-lived charge separated states in nanostructured semiconductor photoelectrodes for the production of solar fuels. Chem. Soc. Rev. 42: 2281–2293.

Das, J. and D. Khushalani. 2010. Nonhydrolytic route for synthesis of ZnO and its use as a recyclable photocatalyst. J. Phys. Chem. C. 114: 2544–2550.

Davda, R.R., J.W. Shabaker, G.W. Huber, R.D. Cortright and J.A. Dumesic. 2005. A review of catalytic issues and process conditions for renewable hydrogen and alkanes by aqueous-phase reforming of oxygenated hydrocarbons over supported metal catalysts. Appl. Catal. B. 56: 171–186.

Dincer, I. 1999. Environmental impacts of energy. Energy Policy 27: 845–854.

Dong, F., Y. Sun, L. Wu, M. Fu and Z. Wu. 2012. Facile transformation of low cost thiourea into nitrogen-rich graphitic carbon nitride nanocatalyst with high visible light photocatalytic performance. Catal. Sci. Technol. 2: 1332–1335.

Dresselhaus, M.S. and I.L. Thomas. 2001. Alternative energy technologies. Nature 414: 332–337.

Du, P., J. Schneider, G. Luo, W.W. Brennessel and R. Eisenberg. 2009. Visible light-driven hydrogen production from aqueous protons catalyzed by molecular cobaloxime catalysts. Inorg. Chem. 48: 4952–4962.

Dukovic, G., B.E. White, Z. Zhou, F. Wang, S. Jockusch, M.L. Steigerwald et al. 2004. Perovskites as catalysts in the reforming of hydrocarbons: a review. J. Am. Chem. Soc. 126: 15269–15275.

Eda, G., C. Mattevi, H. Yamaguchi, H. Kim and M. Chhowalla. 2009. Insulator to semimetal transition in graphene oxide. J. Phys. Chem. C 113: 15768–15771.

Fabre, B., S. Cordier, Y. Molard, C. Perrin, S.A.-Girard and C. Godet. 2009. Electrochemical and charge transport behavior of molybdenum-based metallic cluster layers immobilized on modified n-and p-type Si (111) surfaces. J. Phys. Chem. C 113: 17437–17446.

Felderhoff, M., C. Weidenthaler, R.V. Helmolt and U. Eberle. 2007. Hydrogen storage: the remaining scientific and technological challenges. Phys. Chem. Chem. Phys. 9: 2643–2653.

Feng, X., J.D. Sloppy, T.J. LaTempa, M. Paulose, S. Komarneni, N. Bao et al. 2011. Synthesis and deposition of ultrafine Pt nanoparticles within high aspect ratio TiO_2 nanotube arrays: application to the photocatalytic reduction of carbon. J. Mater. Chem. 21: 13429–13433.

Fernando, K.A.S., S. Sahu, Y. Liu, W.K. Lewis, E.A. Guliants, A. Jafariyan et al. 2015. Carbon quantum dots and applications in photocatalytic energy conversion. ACS Appl. Mater. Interfaces 7: 8363–8376.

Fujishima, A. and K. Honda. 1971. Electrochemical evidence for the mechanism of the primary stage of photosynthesis. Nature 44: 1148–1150.

Fujishima, A. and K. Honda. 1972. Electrochemical photolysis of water at a semiconductor electrode. Nature 238: 37–38.

Ganesh, I. 2014. Conversion of carbon dioxide into methanol—a potential liquid fuel: Fundamental challenges and opportunities (a review). Renew. Sustainable Energy Rev. 31: 221–257.

Ge, L., C.C. Han and J. Liu. 2011. Novel visible light-induced gC_3N_4/Bi_2WO_6 composite photocatalysts for efficient degradation of methyl orange. Appl. Catal. B 108-109: 100−107.

Georgekutty, R., M.K. Seery and S.C. Pillai. 2008. A highly efficient Ag-ZnO photocatalyst: synthesis, properties, and mechanism. J. Phys. Chem. C 112: 13563–13570.

Giesekam, J., J. Barrett, P. Taylor and A. Owen. 2014. The greenhouse gas emissions and mitigation options for materials used in UK construction. Energy Build. 78: 202–214.

Gouedard, V.B., G. Rimmele, O. Porcherie, N. Quisel and J. Desroches. 2009. A solution against well cement degradation under CO_2 geological storage environment. Int. J. Greenhouse Gas Control. 3: 206–216.

Gusain, R., P. Kumar, O.P. Sharma, S.L. Jain and O.P. Khatri. 2016. Reduced graphene oxide–CuO nanocomposites for photocatalytic conversion of CO_2 into methanol under visible light irradiation. Appl. Catal. B 181: 352–362.

Halmann, M. 1978. Photoelectrochemical reduction of aqueous carbon dioxide on p-type gallium phosphide in liquid junction solar cells. Nature 275: 115–116.

Hashimoto, K., H. Irie and A. Fujishima. 2005. TiO_2 photocatalysis: a historical overview and future prospects. Jpn. J. Appl. Phys. 44: 8269–8285.

He, Y., L. Zhang, B. Teng and M. Fan. 2015. New application of Z-scheme $Ag_3PO_4/g\text{-}C_3N_4$ composite in converting CO_2 to fuel. Environ. Sci. Technol. 49: 649–656.

Hochbaum, A.I. and P. Yang. 2010. Semiconductor nanowires for energy conversion. Chem. Rev. 110: 527–546.

Hong, J., X. Xia, Y. Wang and R. Xu. 2012. Mesoporous carbon nitride with *in situ* sulfur doping for enhanced photocatalytic hydrogen evolution from water under visible light. J. Mater. Chem. 22: 15006–15012.

Hong, J., W. Zhang, Y. Wang, T. Zhou and R. Xu. 2014. Photocatalytic reduction of carbon dioxide over self-assembled carbon nitride and layered double hydroxide: the role of carbon dioxide enrichment. ChemCatChem. 6: 2315–2321.

Hou, J., Z. Wang, W. Kan, S. Jiao, H. Zhu and R.V. Kumar. 2012. Efficient visible-light-driven photocatalytic hydrogen production using CdS@TaON core–shell composites coupled with graphene oxide nanosheets. J. Mater. Chem. 22: 7291–7299.

Hsu, H.C., I. Shown, H.Y. Wei, Y.C. Chang, H.Y. Du, Y.G. Lin et al. 2013. Graphene oxide as a promising photocatalyst for CO_2 to methanol conversion. Nanoscale 5: 262–268.

Hu, Y.H., H. Wang and B. Hu. 2010. Thinnest two-dimensional nanomaterial—graphene for solar energy. ChemSusChem. 3: 782–796.

Hummers, W.S. and R.E. Offeman. 1958. Preparation of graphitic oxide. J. Am. Chem. Soc. 80: 1339.

In, S., D.D. Vaughn and R.E. Schaak. 2012. Photocatalytic conversion of CO_2 in water over layered double hydroxides. Angew. Chem. 124: 3981–3984.

Inoue, T., A. Fujishima, S. Konishi and K. Honda. 1979. Photoelectrocatalytic reduction of carbon dioxide in aqueous suspensions of semiconductor powders. Nature 277: 637–638.

Iwase, A., Y.H. Ng, Y. Ishiguro, A. Kudo and R. Amal. 2011. Reduced graphene oxide as a solid-state electron mediator in Z-scheme photocatalytic water splitting under visible light. J. Am. Chem. Soc. 133: 11054–11057.

Izumi, Y. 2013. Recent advances in the photocatalytic conversion of carbon dioxide to fuels with water and/or hydrogen using solar energy and beyond. Coord. Chem. Rev. 257: 171–186.

Jacobson, M.Z., R.W. Howarth, M.A. Delucchi, S.R. Scobie, J.M. Barth, M.J. Dvorak et al. 2013. Examining the feasibility of converting New York State's all-purpose energy infrastructure to one using wind, water, and sunlight. Energy Policy 57: 585–601.

Jensen, L.L., J.T. Muckerman and M.D. Newton. 2008. First-principles studies of the structural and electronic properties of the $(Ga_{1-x}Zn_x)(N_{1-x}O_x)$ solid solution photocatalyst. J. Phys. Chem. C 112: 3439–3446.

Ji, Z., X. Shen, G. Zhu, H. Zhou and A. Yuan. 2012. Reduced graphene oxide/nickel nanocomposites: facile synthesis, magnetic and catalytic properties. J. Mater. Chem. 22: 3471–3477.

Johnson, J.M.F., A.J. Franzluebbers, S.L. Weyers and D.C. Reicosky. 2007. Agricultural opportunities to mitigate greenhouse gas emissions. Environ. Pollution 150: 107–124.

Kailasam, K., J.D. Epping, A. Thomas, S. Losse and H. Junge. 2011. Mesoporous carbon nitride–silica composites by a combined sol–gel/thermal condensation approach and their application as photocatalysts. Energy Environ. Sci. 4: 4668–4674.

Kailasam, K., A. Fischer, G. Zhang, J. Zhang, M. Schwarze, M. Schrçder et al. 2015. Mesoporous carbon nitride-tungsten oxide composites for enhanced photocatalytic hydrogen evolution. ChemSusChem. 8: 1404–1410.

Karamian, E. and S. Sharifnia. 2016. On the general mechanism of photocatalytic reduction of CO_2. Journal of CO_2 Utilization 16: 194–203.

Kato, H. and A. Kudo. 2003. Photocatalytic water splitting into H_2 and O_2 over various tantalate photocatalysts. Catal. Today 78: 561–569.

Kibsgaard, J., T.F. Jaramillo and F. Besenbacher. 2014. Building an appropriate active-site motif into a hydrogen-evolution catalyst with thiomolybdate $[Mo_3S_{13}]^{2-}$ clusters. Nat. Chem. 6: 248–253.

Kondratenko, E.V., G. Mul, J. Baltrusaitis, G.O. Larrazabal and J.P. Ramırez. 2013. Status and perspectives of CO_2 conversion into fuels and chemicals by catalytic, photocatalytic and electrocatalytic processes. Energy Environ. Sci. 6: 3112–3135.

Konta, R., T. Ishii, H. Kato and A. Kudo. 2004. Photocatalytic activities of noble metal ion doped $SrTiO_3$ under visible light irradiation. J. Phys. Chem. B 108: 8992.

Krol, R., Y. Liang and J. Schoonman. 2008. Solar hydrogen production with nanostructured metal oxides. J. Matter. Chem. 18: 2311–2320.

Kumar, B., M. Llorente, J. Froehlich, T. Dang, A. Sathrum and C.P. Kubiak. 2012. Photochemical and photoelectrochemical reduction of CO_2. Annu. Rev. Phys. Chem. 63: 541–69.

Kumar, P., A. Kumar, B. Sreedhar, B. Sain, S.S. Ray and S.L. Jain. 2014a. Cobalt phthalocyanine immobilized on graphene oxide: An efficient visible-active catalyst for the photoreduction of carbon dioxide. Chem. Eur. J. 20: 6154–61611.

Kumar, P., B. Sain and S.L. Jain. 2014b. Photocatalytic reduction of carbon dioxide to methanol using a ruthenium trinuclear polyazine complex immobilized on graphene oxide under visible light. J. Mater. Chem. A 2: 11246–11253.

Kumar, P., S. Kumar, S. Cordier, S. Paofai, R. Boubherroub and S.L. Jain. 2014c. Photoreduction of CO_2 to methanol with hexanuclear molybdenum $[Mo_6Br_{14}]^{2-}$ cluster units under visible light irradiation. RSC Adv. 4: 10420–10423.

Kumar, P., A. Kumar, C. Joshi, R. Singh, S. Saran and S.L. Jain. 2015a. Heterostructured nanocomposite tin phthalocyanine@mesoporous ceria (SnPc@CeO_2) for photoreduction of CO_2 in visible light. RSC Adv. 5: 42414–42421.

Kumar, P., R.K. Chauhan, B. Sain and S.L. Jain. 2015b. Photo-induced reduction of CO_2 using a magnetically separable Ru-CoPc@TiO_2@SiO_2@Fe_3O_4 catalyst under visible light irradiation. Dalton Trans. 44: 4546–4553.

Kumar, P., C. Joshi, N. Labhsetwar, R. Boukherroub and S.L. Jain. 2015c. A novel Ru/TiO_2 hybrid nanocomposite catalyzed photoreduction of CO_2 to methanol under visible light. Nanoscale 7: 15258–15267.

Kumar, P., A. Bansiwal, N. Labhsetwar and S.L. Jain. 2015d. Visible light assisted photocatalytic reduction of CO_2 using a graphene oxide supported heteroleptic ruthenium complex. Green Chem. 17: 1605–1609.

Kumar, P., H.P. Mungse, O.P. Khatri and S.L. Jain. 2015e. Nitrogen-doped graphene-supported copper complex: a novel photocatalyst for CO_2 reduction under visible light irradiation. RSC Adv. 5: 54929–54935.

Kumar, P., H.P. Mungse, S. Cordier, R. Boukherroub, O.P. Khatri and S.L. Jain. 2015f. Hexamolybdenum clusters supported on graphene oxide: Visible-light induced photocatalytic reduction of carbon dioxide into methanol. Carbon 94: 91–100.

Kumar, P., N.G. Naumov, R. Boukherroub and S.L. Jain. 2015g. Octahedral rhenium $K_4[Re_6S_8(CN)_6]$ and $Cu(OH)_2$ cluster modified TiO_2 for the photoreduction of CO_2 under visible light irradiation. Appl. Catal. A 499: 32–38.

Kumar, P., A. Kumar, C. Joshi, S. Ponnada, A.K. Pathak, A. Ali et al. 2016. A $[Fe(bpy)_3]^{2+}$ grafted graphitic carbon nitride hybrid for visible light assisted oxidative coupling of benzylamines under mild reaction conditions. Green Chem. 18: 2514–2521.

Kumar, S.G. and L.G. Devi. 2011. Review on modified TiO_2 photocatalysis under UV/visible light: selected results and related mechanisms on interfacial charge carrier transfer dynamics. J. Phys. Chem. A 115: 13211–13241.

Kuriki, R., K. Sekizawa, O. Ishitani and K. Maeda. 2015. Visible-light-driven CO_2 reduction with carbon nitride: enhancing the activity of ruthenium catalysts. Angew. Chem. Int. Ed. 54: 2406–2409.

Kuriki, R., H. Matsunaga, T. Nakashima, K. Wada, A. Yamakata, O. Ishitani et al. 2016. Nature-inspired, highly durable CO_2 reduction system consisting of a binuclear ruthenium (II) complex and an organic semiconductor using visible light. J. Am. Chem. Soc. 138: 5159–5170.

Lanzafame, P., G. Centi and S. Perathoner. 2014. Catalysis for biomass and CO_2 use through solar energy: opening new scenarios for a sustainable and low-carbon chemical production. Chem. Soc. Rev. 43: 7562–7580.

Lee, D.-S., H.-J. Chen and Y.-W. Chen. 2012. Photocatalytic reduction of carbon dioxide with water using $InNbO_4$ catalyst with NiO and Co_3O_4 cocatalysts. J. Physics and Chemistry of Solids 73: 661–669.

Li, J. and D. Xu. 2010. Tetragonal faceted-nanorods of anatase TiO_2 single crystals with a large percentage of active {100} facets. Chem. Commun. 46: 2301–2303.

Li, J., K. Cao, Q. Li and D. Xu. 2012. Tetragonal faceted-nanorods of anatase TiO_2 with a large percentage of active {100} facets and their hierarchical structure. CrystEngComm. 14: 83–85.

Li, K., X. An, K.H. Park and M. Khrasheh. 2014. A critical review of CO_2 photoconversion: catalysts and reactors. Catal. Today 224: 3–12.

Li, M., L. Zhang, X. Fan, M. Wu, M. Wang, R. Cheng et al. 2017. Core-shell $LaPO_4/gC_3N_4$ nanowires for highly active and selective CO_2 reduction. Appl. Catal. B 201: 629–635.

Li, R., Z. Chen, W. Zhao, F. Zhang, K. Maeda, B. Huang et al. 2013a. Sulfurization-assisted cobalt deposition on $Sm_2Ti_2S_2O_5$ photocatalyst for water oxidation under visible light irradiation. J. Phys. Chem. C 117: 376–382.

Li, X., Q. Wang, Y. Zhao, W. Wu, J. Chen and H. Meng. 2013b. Green synthesis and photo-catalytic performances for ZnO-reduced graphene oxide nanocomposites. J. Colloid Interface Sci. 411: 69–75.

Liang, Y.T., B.K. Vijayan, K.A. Gray and M.C. Hersam. 2011. Minimizing graphene defects enhances titania nanocomposite-based photocatalytic reduction of CO_2 for improved solar fuel production. Nano Lett. 11: 2865–2870.

Liang, Y.T., B.K. Vijayan, O. Lyandres, K.A. Gray and M.C. Hersam. 2012. Effect of dimensionality on the photocatalytic behavior of carbon–titania nanosheet composites: charge transfer at nanomaterial interfaces. J. Phys. Chem. Lett. 3: 1760–1765.

Lin, Z., G. Waller, Y. Liu, M. Liu and C.P. Wong. 2012. Facile synthesis of nitrogen-doped graphene via pyrolysis of graphene oxide and urea, and its electrocatalytic activity toward the oxygen-reduction reaction. Adv. Energy Mater. 2: 884–888.

Lin, J., Z. Pan and X. Wang. 2014. Photochemical reduction of CO_2 by graphitic carbon nitride polymers. ACS Sustainable Chem. Eng. 2: 353−358.

Linsebigler, A.L., G. Lu and J.T. Yates, Jr. 1995. Photocatalysis on TiO_2 surfaces: principles, mechanisms, and selected results. Chem. Rev. 95: 735–758.

Liu, G., C. Sun, H.G. Yang, S.C. Smith, L. Wang, G.Q. Lu et al. 2010a. Nanosized anatase TiO_2 single crystals for enhanced photocatalytic activity. Chem. Commun. 46: 755–757.

Liu, J., Z. Zhao, C. Xu, A. Duan and G. Jiang. 2010b. Simultaneous removal of soot and NOx over the $(La_{1.7}Rb_{0.3}CuO_4)x/nmCeO_2$ nanocomposite catalysts. Ind. Eng. Chem. Res. 49: 3112–3119.

Liu, Q., Y. Zhou, J. Kou, X. Chen, Z. Tian, J. Gao et al. 2010c. High-yield synthesis of ultralong and ultrathin Zn_2GeO_4 nanoribbons toward improved photocatalytic reduction of CO_2 into renewable hydrocarbon fuel. J. Am. Chem. Soc. 132: 14385–14387.

Liu, S., J. Yu and M. Jaroniec. 2010d. Tunable photocatalytic selectivity of hollow TiO_2 microspheres composed of anatase polyhedra with exposed {001} facets. J. Am. Chem. Soc. 132: 11914–11916.

Liu, S., J. Yu and M. Jaroniec. 2011. Anatase TiO_2 with dominant high-energy {001} facets: synthesis, properties, and applications. Chem. Mater. 23: 4085–4093.

Liu, X., H. Zhang, X. Yao, T. An, P. Liu, Y. Wang et al. 2012. Visible light active pure rutile TiO_2 photoanodes with 100% exposed pyramid-shaped (111) surfaces. Nano Res. 5: 762–769.

Loh, K.P., Q. Bao, G. Eda and M. Chhowalla. 2010. Graphene oxide as a chemically tunable platform for optical applications. Nature Chem. 2: 1015–1024.

Low, J., J. Yu and W. Ho. 2015. Graphene-based photocatalysts for CO_2 reduction to solar fuel. J. Phys. Chem. Lett. 6: 4244–4251.

Manne, A.S. and R.G. Richels. 2001. An alternative approach to establishing trade-offs among greenhouse gases. Nature 401: 675–677.

Mao, J., K. Li and T. Peng. 2013. Recent advances in the photocatalytic CO_2 reduction over semiconductors. Catal. Sci. Technol. 3: 2481–2498.

Markewitz, P., W. Kuckshinrichs, W. Leitner, J. Linssen, P. Zapp, R. Bongartz et al. 2012. Worldwide innovations in the development of carbon capture technologies and the utilization of CO_2. Energy Environ. Sci. 5: 7281–7305.

Mohamed, H.H. and D.W. Bahnemann. 2012. The role of electron transfer in photocatalysis: Fact and fictions. App. Cat. B 128: 91–104.

Momirlan, M. and T. Veziroglu. 2005. The properties of hydrogen as fuel tomorrow in sustainable energy system for a cleaner planet. Int. J. Hyrdo. Energy 30: 795–802.

Nagaveni, K., M.S. Hegde, N. Ravishankar, G.N. Subbanna and G. Madras. 2004. Synthesis and structure of nanocrystalline TiO_2 with lower band gap showing high photocatalytic activity. Langmuir 20: 2900–2907.

Navalon, S., A. Dhakshinamoorthy, M. Alvaro and H. Garcia. 2013. Photocatalytic CO_2 reduction using non-titanium metal oxides and sulfides. ChemSusChem. 6: 562–577.

Neaţu, S., J.A. M.-Agullo and H. Garcia. 2014. Solar light photocatalytic CO_2 reduction: general considerations and selected bench-mark photocatalysts. Int. J. Mol. Sci. 15: 5246–5262.

Novoselov, K.S., A.K. Geim, S.V. Morozov, D. Jiang, Y. Zhang, S.V. Dubonos et al. 2004. Electric field effect in atomically thin carbon films. Science 306: 666–669.

Olah, G.A., A. Goeppert and G.K.S. Prakash. 2009. Chemical recycling of carbon dioxide to methanol and dimethyl ether: From greenhouse gas to renewable, environmentally carbon neutral fuels and synthetic hydrocarbons. J. Org. Chem. 74: 487–498.

Ong, W.-J., L.-L. Tan, S.-P. Chail, S.-T. Yong and A.R. Mohamed. 2014. Self-assembly of nitrogen-doped TiO_2 with exposed {001} facets on a graphene scaffold as photo-active hybrid nanostructures for reduction of carbon dioxide to methane. Nano Res. 7: 1528–1547.

Ong, W.-J., L.-L. Tan, Y.H. Ng, S.-T. Yong and S.-P. Chai. 2016. Graphitic carbon nitride $(g\text{-}C_3N_4)$-based photocatalysts for artificial photosynthesis and environmental remediation: are we a step closer to achieving sustainability? Chem. Rev. 116: 7159–7329.

Pan, C.S., J. Xu, Y.J. Wang, D. Li and Y.F. Zhu. 2012. Dramatic activity of $C_3N_4/BiPO_4$ photocatalyst with core/shell structure formed by self-assembly. Adv. Funct. Mater. 22: 1518−1524.

Pan, F., K. Wu, H. Li, G. Xu, and W. Chen. 2014. Synthesis of {100} facet dominant anatase TiO_2 nanobelts and the origin of facet-dependent photoreactivity. Chem. Eur. J. 20: 15095–15101.

Pan, P.-W. and Y.-W. Chen. 2007. Photocatalytic reduction of carbon dioxide on NiO/$InTaO_4$ under visible light irradiation. Catal. Commun. 8: 1546–1549.
Panwar, N.L., S.C. Kaushik and S. Kothari. 2011. Role of renewable energy sources in environmental protection: a review. Renew. Sustain. Energy Rev. 15: 1513–1524.
Park, H., J.H. Choi, K.M. Choi, D.K. Lee and J.K. Kang. 2012. Highly porous gallium oxide with a high CO_2 affinity for the photocatalytic conversion of carbon dioxide into methane. J. Mater. Chem. 22: 5304.
Peharz, G., F. Dimorth and U. Wittstadt. 2007. Solar hydrogen production by water splitting with a conversion efficiency of 18%. Int. J. Hydro. Energy 32: 3248–3252.
Peura, P. and T. Hyttinin. 2011. The potential and economics of bioenergy in Finland. J. Cleaner Pro. 19: 927–945.
Portehault, D., C. Giordano, C. Gervais, I. Senkovska, S. Kaskel, C. Sanchez et al. 2010. High-surface-area nanoporous boron carbon nitrides for hydrogen storage. Adv. Funct. Mater. 20: 1827–1833.
Powell, T.W.R. and T.M. Lenton. 2012. Future carbon dioxide removal via biomass energy constrained by agricultural efficiency and dietary trends. Energy Environ. Sci. 5: 8116–8133.
Pradhan, N. and D.D. Sharma. 2011. Advances in light-emitting doped semiconductor nanocrystals. J. Phys. Chem. Lett. 2: 2818–2826.
Qu, Y. and X. Duan. 2013. Progress, challenge and perspective of heterogeneous photocatalysts. Chem. Soc. Rev. 42: 2568–2580.
Rao, C.N.R., K. Biswas, K.S. Subrahmanyama and A. Govindaraj. 2009. Graphene, the new nanocarbon. J. Mater. Chem. 19: 2457–2469.
Rehan, R. and M. Nehdi. 2005. Carbon dioxide emissions and climate change: policy implications for the cement industry. Environ. Sci. Policy 8: 105–114.
Roy, S.C., O.K. Varghese, M. Paulose and C.A. Grimes. 2010. Toward solar fuels: photocatalytic conversion of carbon dioxide to hydrocarbons. ACS Nano 4: 1259–1278.
Sahoo, N.G., Y. Pan, L. Li and S.H. Chan. 2012. Graphene-based materials for energy conversion. Adv. Mater. 24: 4203–4210.
Sahu, S., Y. Liu, P. Wang, C.E. Bunker, K.A.S. Fernando, W.K. Lewis et al. 2014. Visible-light photoconversion of carbon dioxide into organic acids in an aqueous solution of carbon dots. Langmuir 30: 8631–8636.
Sato, S., T. Arai and T. Morikawa. 2015. Toward solar-driven photocatalytic CO_2 reduction using water as an electron donor. Inorg. Chem. 54: 5105–5113.
Sekizawa, K., K. Maeda, K. Domen, K. Koike and Osamu Ishitani. 2013. Artificial Z-scheme constructed with a supramolecular metal complex and semiconductor for the photocatalytic reduction of CO_2. J. Am. Chem. Soc. 135: 4596–4599.
Serpone, N., D. Lawless and R. Khairutdinov. 1995. Size effects on the photophysical properties of colloidal anatase TiO_2 particles: size quantization versus direct transitions in this indirect semiconductor? J. Phys. Chem. 99: 16646–16654.
Shi, H., G. Chen, C. Zhang and Z. Zou. 2014. Polymeric g-C_3N_4 coupled with $NaNbO_3$ nanowires toward enhanced photocatalytic reduction of CO_2 into renewable fuel. ACS Catal. 4: 3637–3643.
Shown, I., H.C. Hsu, Y.C. Chang, C.H. Lin, P.K. Roy, A. Ganguly et al. 2014. Highly efficient visible light photocatalytic reduction of CO_2 to hydrocarbon fuels by Cu-nanoparticle decorated graphene oxide. Nano Lett. 14: 6097−6103.
Sun, L., Y. Qin, Q. Cao, B. Hu, Z. Huang, L. Ye et al. 2011. Novel photocatalytic antibacterial activity of TiO_2 microspheres exposing 100% reactive {111} facets. Chem. Commun. 47: 12628–12630.
Tahir, M. and N.S. Amin. 2013. Advances in visible light responsive titanium oxide-based photocatalysts for CO_2 conversion to hydrocarbon fuels. Energy Convers. Manage 76: 194–214.
Takanabe, K., K. Kamata, X. Wang, M. Antonietti, J. Kubota and K. Domen. 2010. Photocatalytic hydrogen evolution on dye-sensitized mesoporous carbon nitride photocatalyst with magnesium phthalocyanine. Phys. Chem. Chem. Phys. 12: 13020–13025.
Takanabe, K. and K. Domen. 2012. Preparation of inorganic photocatalytic materials for overall water splitting. ChemCatChem. 4: 1–14.
Takayama, T., K. Sato, T. Fujimura, Y. Kojima, A. Iwase and A. Kudo. 2017. Photocatalytic CO_2 reduction using water as an electron donor by a powdered Z-scheme system consisting of metal sulfide and an RGO–TiO_2 composite. Faraday Discuss 198: 397–407.
Tan, L.-L., W.-J. Ong, S.-P. Chai and A.R. Mohamed. 2013. Reduced graphene oxide-TiO_2 nanocomposite as a promising visible-light-active photocatalyst for the conversion of carbon dioxide. Nanoscale Res. Lett. 8: 465.
Tan, L.-L., W.-J. Ong, S.-P. Chai, B.T. Goh and A.R. Mohamed. 2015a. Visible-light-active oxygen-rich TiO_2 decorated 2D graphene oxide with enhanced photocatalytic activity toward carbon dioxide reduction. Appl. Catal. B 179: 160–170.
Tan, L.-L., W.-J. Ong, S.-P. Chai and A.R. Mohamed. 2015b. Noble metal modified reduced graphene oxide/TiO_2 ternary nanostructures for efficient visible-light-driven photoreduction of carbon dioxide into methane. Appl. Catal. B 166–167: 251–259.
Teramura, K., S. Iguchi, Y. Mizuno, T. Shishido and T. Tanaka. 2012. Photocatalytic conversion of CO_2 in water over layered double hydroxides. Angew Chem. Int. Ed. 51: 8001–8018.
Tsai, C.W., H.M. Chen, R.S. Liu, K. Asakura and T.S. Chan. 2011. Ni@NiO core–shell structure-modified nitrogen-doped $InTaO_4$ for solar-driven highly efficient CO_2 reduction to methanol. J. Phys. Chem. C 115: 10180–10186.
Tseng, I.-H., J.C.S. Wu and H.-Y. Chou. 2004. Effects of sol–gel procedures on the photocatalysis of Cu/TiO_2 in CO_2 photoreduction. J. Catal. 221: 432–440.
Varghese, O.K., M. Paulose, T.J. Latempa and C.A. Grimes. 2009. High-rate solar photocatalytic conversion of CO_2 and water vapor to hydrocarbon fuels. Nano Lett. 9: 731–737.

Wang, C., R.L. Thompson, J. Baltrus and C. Matranga. 2010. Visible light photoreduction of CO_2 using CdSe/Pt/TiO_2 heterostructured catalysts. J. Phys. Chem. Lett. 1: 48–53.

Wang, J., D.N. Tafen, J.P. Lewis, Z. Hong, A. Manivannan, M. Zhi et al. 2009a. Origin of photocatalytic activity of nitrogen-doped TiO_2 nanobelts. J. Am. Chem. Soc. 131: 12290–12297.

Wang, J.C., L. Zhang, W.-X. Fang, J. Ren, Y.-Y. Li, H.-C. Yao et al. 2015a. Enhanced photoreduction CO_2 activity over direct Z-scheme α-Fe_2O_3/Cu_2O heterostructures under visible light irradiation. ACS Appl. Mater. Interfaces 7: 8631–8639.

Wang P.-Q., Y. Bai, P.-Y. Luo and J.-Y. Liu. 2013b. Graphene–WO3 nanobelt composite: Elevated conduction band toward photocatalytic reduction of CO_2 into hydrocarbon fuels. Catal. Commun. 38: 82–85.

Wang, W., S. Wang, X. Ma and J. Gong. 2011. Recent advances in catalytic hydrogenation of carbon dioxide. Chem. Soc. Rev. 40: 3703–3727.

Wang, X., K. Maeda, X. Chen, K. Takanabe, K. Domen, Y. Hou et al. 2009b. Polymer semiconductors for artificial photosynthesis: hydrogen evolution by mesoporous graphitic carbon nitride with visible light. J. Am. Chem. Soc. 131: 1680–1681.

Wang, Y., Q. Wang, X. Zhan, F. Wang, M. safdar and J. He. 2013a. Visible light driven type II heterostructures and their enhanced photocatalysis properties: a review. Nanoscle 5: 8326–8339.

Wang, Z.W., Y. Yue and Y. Cao. 2014. Preparation and properties of nitrogen doped p-type zinc oxide films by reactive magnetron sputtering. Vacuum 101: 313–316.

Wang, Z., G. Liu, C. Ding, Z. Chen, F. Zhang, J. Shi et al. 2015b. Synergetic effect of conjugated $Ni(OH)_2$/IrO_2 cocatalyst on titanium-doped hematite photoanode for solar water splitting. J. Phys. Chem. C 119: 19607–19612.

Wehling, T.O., K.S. Novoselov, S.V. Morozov, E.E. Vdovin, M.I. Katsnelson, A.K. Giem et al. 2008. Molecular doping of grapheme. Nano. Lett. 8: 173–177.

Woolerton, T.W., S. Sheard, E. Reisner, E. Pirece, S.W. Ragsdale and F.A. Armstrong. 2010. Efficient and clean photoreduction of CO_2 to CO by enzyme-modified TiO_2 nanoparticles using visible light. J. Am. Chem. Soc. 132: 2132–2133.

Wu, J., R.M. Yadav, M. Liu, P.P. Sharma, C.S. Tiwary, L. Ma et al. 2015. Achieving highly efficient, selective, and stable CO_2 reduction on nitrogen-doped carbon nanotubes. ACS Nano 9: 5364–5371.

Xiang, Q., J. Yu, W. Wang and M. Jaroniec. 2011. Nitrogen self-doped nanosized TiO_2 sheets with exposed {001} facets for enhanced visible-light photocatalytic activity. Chem. Commun. 47: 6906–6908.

Xie, S., Y. Wang, Q. Zhang, W. Deng and Y. Wang. 2015. $SrNb_2O_6$ nanoplates as efficient photocatalysts for the preferential reduction of CO_2 in the presence of H_2O. Chem. Commun. 51: 3430–3433.

Xing, M., F. Shen, B. Qiu and J. Zhang. 2014. Highly-dispersed boron-doped graphene nanosheets loaded with TiO_2 nanoparticles for enhancing CO_2 photoreduction. Sci. Rep. 4: 6341.

Xu, H., P. Reunchan, S. Ouyang, H. Tong, N. Umezawa, T. Kako et al. 2013a. Anatase TiO_2 single crystals exposed with high-reactive {111} facets toward efficient H_2 evolution. Chem. Mater. 25: 405–411.

Xu, H., S. Ouyang, P. Li, T. Kako and J. Ye. 2013b. High-active anatase TiO_2 nanosheets exposed with 95% {100} facets toward efficient H_2 evolution and CO_2 photoreduction. ACS Appl. Mater. Interfaces 5: 1348–1354.

Xu, J., Y. Wang and Y. Zhu. 2013c. Nanoporous graphitic carbon nitride with enhanced photocatalytic performance. Langmuir 29: 10566–10572.

Yadav, D., R.K. Yadav, A. Kumar, N.-J. Park and J.-O. Baeg. 2016. Functionalized graphene quantum dots as efficient visible-light photocatalysts for selective solar fuel production from CO_2. Chemcatchem. 8: 3389–3393.

Yamanaka, K.I., S. Sato, M. Iwaki, T. kajino and T. Morikawa. 2011. Photoinduced electron transfer from nitrogen-doped tantalum oxide to adsorbed ruthenium complex. J. Phys. Chem. C 115: 18348–18353.

Yan, S.C., S.B. Lv, Z.S. Li and Z.G. Zou. 2010. Organic–inorganic composite photocatalyst of gC_3N_4 and TaON with improved visible light photocatalytic activities. Dalton Trans. 39: 1488−1491.

Yan, S., H. Yu, N. Wang, Z. Li and Z. Zou. 2012. Efficient conversion of CO_2 and H_2O into hydrocarbon fuel over $ZnAl_2O_4$-modified mesoporous ZnGaNO under visible light irradiation. Chem. Commun. 48: 1048–1050.

Yang, H.G., C.H. Sun, S.Z. Qiao, J. Zou, G. Liu, S.C. Smith et al. 2008. Anatase TiO_2 single crystals with a large percentage of reactive facets. Nature 453: 638–641.

Yang, H.G., G. Liu, S.Z. Qiao, C.H. Sun, Y.G. Jin, S.C. Smith et al. 2009. Solvothermal synthesis and photoreactivity of anatase TiO_2 nanosheets with dominant {001} facets. J. Am. Chem. Soc. 131: 4078–4083.

Yang, M.Q., N. Zhang, M. Pagliaro and Y.J. Xu. 2014. Artificial photosynthesis over graphene–semiconductor composites. Are we getting better? Chem. Soc. Rev. 43: 8240–8254.

Yang, S., D. Prendergast and J.B. Neaton. 2012. Tuning semiconductor band edge energies for solar photocatalysis via surface ligand passivation. Nano Lett. 12: 383–388.

Yeh, T.-F., J.-M. Syu, C. Cheng, T.-H. Chang and H. Teng. 2010. Graphite oxide as a photocatalyst for hydrogen production from water. Adv. Funct. Mater. 20: 2255–2262.

Yu, J. and J. Ran. 2011. Facile preparation and enhanced photocatalytic H_2-production activity of $Cu(OH)_2$ cluster modified TiO_2. Energy Environ. Sci. 4: 1364–1371.

Yu, J., J. Low, W. Xiao, P. Zhou and M. Jaroniec. 2014a. Enhanced photocatalytic CO_2-reduction activity of anatase TiO_2 by coexposed {001} and {101} facets. J. Am. Chem. Soc. 136: 8839–8842.

Yu, J., J. Jin, B. Cheng and M. Jaroniec. 2014b. A noble metal-free reduced graphene oxide–CdS nanorod composite for the enhanced visible-light photocatalytic reduction of CO_2 to solar fuel. J. Mater. Chem. A. 2: 3407–3416.

Yu, Q., Y. Wang, Z. Yi, N. Zu, J. Zhang, M. Zhang et al. 2010. High-efficiency dye-sensitized solar cells: the influence of lithium ions on exciton dissociation, charge recombination, and surface states. ACS Nano 4: 6032–6038.

Zachos, J.C., G.R. Dickens and R.E. Zeebe. 2008. An early Cenozoic perspective on greenhouse warming and carbon-cycle dynamics. Nature 451: 279–283.

Zhang, G., M. Zhang, X. Ye, X. Qiu, S. Lin and X. Wang. 2014. Iodine modified carbon nitride semiconductors as visible light photocatalysts for hydrogen evolution. Adv. Mater. 26: 805–809.

Zhang, N., Y. Zhang and Y.-J. Xu. 2012. Recent progress on graphene-based photocatalysts: current status and future perspectives. Nanoscale 4: 5792–5813.

Zhang, Q., J. Wang, S. Yin, T. Sato and F. Saito. 2004. Synthesis of a visible-light active $TiO_{2-x}S_x$ photocatalyst by means of mechanochemical doping. J. Am. Ceram. Soc. 126: 1161–1163.

Zhang, Q., Y. Li, E.A. Ackerman, M.G. Josifovska and H. Li. 2011a. Visible light responsive iodine-doped TiO_2 for photocatalytic reduction of CO_2 to fuels. Appl. Catal. A 400: 195–202.

Zhang, Q., Y. Li, E.A. Ackerman, M.G. Josifovska and H. Li. 2011b. Visible light responsive iodine-doped TiO_2 for photocatalytic reduction of CO_2 to fuels. Appl. Catal. A 400: 195–202.

Zhang, Y., T. Mori, J. Ye and M. Antonietti. 2010. Phosphorus-doped carbon nitride solid: enhanced electrical conductivity and photocurrent generation. J. Am. Chem. Soc. 132: 6294–6295.

Zhang, Z., Z. Wang, S.-W. Cao and C. Xue. 2013. Au/Pt nanoparticle-decorated TiO_2 nanofibers with plasmon-enhanced photocatalytic activities for solar-to-fuel conversion. J. Phys. Chem. C 117: 25939–25947.

Zhao, Z., J. Fan, M. Xie and Z. Wang. 2009. Photo-catalytic reduction of carbon dioxide with *in situ* synthesized $CoPc/TiO_2$ under visible light irradiation. J. Clean. Prod. 17: 1025–1029.

Zhong, D.K., S. Choi and D.R. Gamelin. 2011. Near-complete suppression of surface recombination in solar photoelectrolysis by "Co-Pi" catalyst-modified W: $BiVO_4$. J. Am. Chem. Soc. 133: 18370–18377.

Zhou, C.H., J.N. Beltramini, Y.X. Fan and G.Q. Lu. 2008. Chemoselective catalytic conversion of glycerol as a biorenewable source to valuable commodity chemicals. Chem. Soc. Rev. 37: 527–549.

Zhu, G., Y.V. Geletii, P. Kogerler, H. Schilder, J. Song, S. Lense et al. 2012. Water oxidation catalyzed by a new tetracobalt-substituted polyoxometalate complex: $[\{Co_4(\mu OH)(H_2O)_3\}(Si_2W_{19}O_{70})]^{11-}$. Dalton Trans. 41: 2084–2090.

Zhuang, S., X. Xu, B. Feng, J. Hu, Y. Pang, G. Zhou et al. 2014. Photogenerated carriers transfer in dye–graphene–SnO_2 composites for highly efficient visible-light photocatalysis. ACS Appl. Mater. Interfaces 6: 613−621.

Zong, X., C. Sun, H. Yu, Z.G. Chen, Z. Xing, D. Ye et al. 2013. Activation of photocatalytic water oxidation on N-doped ZnO bundle-like nanoparticles under visible light. J. Phys. Chem. C. 117: 4937–4942.